Journal of Computational Physics 231 (2012) 558–585

Contents lists available at SciVerse ScienceDirect

Journal of Computational Physics

journal homepage: www.elsevier.com/locate/jcp

A non-deteriorating algorithm for computational electromagnetism based on quasi-lacunae of Maxwell's equations ☆

S.V. Petropavlovsky [a], S.V. Tsynkov [b,*]

[a] Department of Applied Mathematics, Financial University under the Government of the Russian Federation, Moscow 125993, Russia
[b] Department of Mathematics, North Carolina State University, Box 8205, Raleigh, NC 27695, USA

ARTICLE INFO

Article history:
Received 7 March 2011
Received in revised form 18 September 2011
Accepted 20 September 2011
Available online 1 October 2011

Keywords:
Propagation of unsteady electromagnetic waves
The Huygens' principle
Aft fronts
Accumulation of charge
Electrostatic field
Numerical solution
Long-time computations
Artificial boundary conditions (ABCs)
Perfectly matched layers (PMLs)
Uniform error bound

ABSTRACT

The performance of many well-known methods used for the treatment of outer boundaries in computational electromagnetism (CEM) may deteriorate over long time intervals. The methods found susceptible to this undesirable phenomenon include some local low order artificial boundary conditions (ABCs), as well as perfectly matched layers (PMLs). We propose a universal algorithm for correcting this problem. It works regardless of either why the deterioration occurs in each particular instance, or how it actually manifests itself (loss of accuracy, loss of stability, etc.). Our algorithm relies on the Huygens' principle in the generalized form, when a non-zero electrostatic solution can be present behind aft fronts of the propagating waves, i.e., inside the lacunae of Maxwell's equations. In this case, we refer to quasi-lacunae as opposed to conventional lacunae, for which the solution behind aft fronts is zero. The use of quasi-lacunae allows us to overcome a key constraint of the previously developed version of our algorithm that was based on genuine lacunae. Namely, the currents that drive the solution no longer have to be solenoidal. Another important development is that we apply the methodology to general non-Huygens' problems.

1. Introduction

The most common way of attaining a finite-dimensional discretization for the numerical simulation of waves propagating over unbounded regions is to truncate the original unbounded domain and set an appropriate artificial boundary condition (ABC) at the resulting outer boundary [1,2]. In doing so, the corresponding finite computational domain usually covers the area where all the phenomena and processes essential for a given formulation take place (e.g., waves generation, absorption, or scattering), whereas its unbounded surrounding region, which is thrown away by truncation, is assumed to represent a less sophisticated medium, say, homogeneous and isotropic. In the simplest case, the computational domain may be surrounded by vacuum. In the literature, this geometric partition is often referred to as the partition between the near field and the far field.

Once the waves leave the finite computational domain, they are not supposed to come back and should no longer affect the near field solution. Accordingly, the role of the ABC is to enforce this behavior in simulations, i.e., to make the outer

☆ Work supported by the US NSF, Grant # DMS-0810963, by the US Air Force, Grants # FA9550-07-1-0170 and # FA9550-10-1-0092, and by the US Army, STTR Contract # W911NF-11-C-0245.

* Corresponding author.
E-mail addresses: SPetropavlovsky@fa.ru (S.V. Petropavlovsky), tsynkov@math.ncsu.edu (S.V. Tsynkov).
URL: http://www.math.ncsu.edu/~stsynkov (S.V. Tsynkov).

0021-9991/$ - see front matter © 2011 Elsevier Inc. All rights reserved.
doi:10.1016/j.jcp.2011.09.019

boundary transparent for all the outgoing waves, and to eliminate the unphysical reflections. For time-dependent problems, it is particularly important that the ABC maintains its non-reflecting properties as the time elapses. Then, we can expect that the solution inside the computational domain will remain close to the corresponding fragment of the original infinite-domain solution (will coincide with it if the ABC is exact).

In the field of computational electromagnetism (CEM), there is a number of established techniques to build the ABCs for Maxwell's equations. In particular, there are popular ABCs that are local in space and time, and are typically derived using asymptotic considerations, e.g., those of Bayliss and Turkel, Engquist and Majda, or Higdon (see the reviews [1,2]). However, some of these techniques, while demonstrating excellent grid truncation properties over limited time intervals, may suffer from a deterioration of performance in long-time computations, especially when implemented in a high order setting. Indeed, the empirical study of [3] demonstrates that the solution obtained using Higdon and Bayliss–Turkel fourth order ABCs in the two-dimensional Cartesian case becomes highly unstable already at moderate computational times; and that the instability most likely arises near the corners of the computational domain. In addition, the analysis of [4] shows the possibility of a logarithmic error growth when the two-dimensional d'Alembert equation is driven by a source that operates continuously in time, and is approximated on a half-plane truncated with high order Engquist–Majda boundary conditions. Susceptibility of local ABCs to long-time error growth is also discussed in [5], where a remedy is proposed based on representing the solution as a linear combination of modes that each propagates and decays.

Another very efficient approach to the absorption of waves at the outer boundaries, the so-called perfectly matched layers (PMLs), may also lead to long-time instabilities. They first appear in the layer and subsequently propagate back into the domain. The original split-field PML by Bérenger [6,7] turns out to be only weakly well-posed, and a linear growth of the split field components inside the PML is possible already at the analytical level. In particular, it has been proven in [8] that a very popular Yee scheme [9] becomes unconditionally unstable in the presence of the PML [6], with the powers of amplification matrices growing linearly as the number of time steps increases.

Subsequent developments gave rise to unsplit PMLs, but the latter have also been found susceptible to gradually developing instabilities. First, the instabilities were predicted theoretically, and then also corroborated experimentally, see, e.g., [10]. In Section 6 of this paper, we show, in particular, how rapid the growth can be in the case of a three-dimensional unsplit Cartesian PML. A systematic computational study of the long-time performance of unsplit PMLs with some commonly used explicit second order schemes can be found in [11].

Several approaches have been proposed in the literature to correct the aforementioned long-time instabilities. However, the "stabilized" versions of Higdon's and Liao's [12, Section 6.5] boundary conditions offered an improved performance but did not eliminate the instability completely [3]. Furthermore, efforts to stabilize higher order ABCs were unsuccessful [13]. And when the stability is achieved, it often compromises the accuracy over the lower end of the frequency spectrum [14].

Stabilization techniques for PMLs include changing the governing equations in the layer [10] and introducing frequency-shifted [15–17] or non-linear [18] PMLs. All these modifications perform well computationally, but theoretically it is not clear whether the modified layer remains perfectly matched or absorbing, in particular, absorbing regardless of the frequency.

The main objective of the current paper is to develop a method that would fully prevent the long-time deterioration of the solution in CEM when it is caused by the outer artificial boundary. In doing so, the key idea is rather not to go deep into what actually causes the problem in each specific case, but have a universal methodology that would work independently of both the type of the ABC (or PML) and the nature of deterioration. We would also want it to be rigorously justified, and to have it preserve all the advantageous properties of a given ABC, such as the degree of transparency for a local method or the matching and absorption properties for a PML. The only assumption we make is that *the chosen ABC or PML should be able to maintain its design characteristics over a relatively short yet reasonable interval of time* (compared to the overall duration of computation).

To achieve our objective of preventing the long-time deterioration, we employ a special time-marching technique based on quasi-lacunae of Maxwell's equations [19]. The notion of quasi-lacunae generalizes that of conventional lacunae in the sense of Petrowsky [20]. Namely, in the case of quasi-lacunae, there may be a steady-state electrostatic solution behind aft fronts of the propagating waves, whereas for genuine lacunae the solution behind the aft fronts is zero (the Huygens' principle). Accordingly, the integration technique developed in this paper generalizes the one that we have constructed previously based on the notion of classical lacunae [21–24].

The original lacunae-based integration of [21–24] applies successfully to various wave propagation problems and allows one to obtain temporally uniform error bounds, which is the main reason why it proves useful for eliminating the long-time deterioration. In particular, we have used it in work [25] for stabilizing the unsplit PMLs. However, its implementation in CEM encounters difficulties related to the nature of the Maxwell equations themselves. Namely, Maxwell's equations have classical lacunae only in a very special case, when the currents that drive the solution are solenoidal, i.e., divergence-free. Therefore, to be able to use the lacunae-based time-marching for Maxwell's equations, one needs to construct the auxiliary divergence-free currents [24]. The key advantage of the method proposed in this paper is that it removes this limitation.

Another important development presented in the current paper is the methodology of stabilizing the ABC (or PML) for general non-Huygens' problems. It requires splitting the original problem into the interior and auxiliary sub-problems.

Whereas this technique was previously employed in [22–24], the stabilization approach of [25] was tested only for the genuine Huygens' formulations.

When splitting the original infinite-domain problem, the resulting interior (sub-)problem is set on the bounded computational domain, whereas its auxiliary counterpart is first considered to be formulated on the entire space, and then truncated by the chosen ABC (or PML). The two problems are connected to each other. Solution to the auxiliary problem (AP) provides the outer boundary data for the interior problem and thus renders its closure. In turn, the AP itself is driven by the source terms that are derived from the solution of the interior problem right next to the boundary.

The advantage of the foregoing split is that the interior problem will now contain all the essential near field components of the original formulation yet it will not need any ABCs. As for the AP, in the simplest CEM setting it is a plain initial value problem for constant coefficient Maxwell's equations. The AP is driven by the prescribed currents and truncated by the chosen ABC or PML. It is much easier to analyze than the original problem. In particular, one can see that if the currents are compactly supported in time, then solution to the AP will have a quasi-lacuna.

The actual currents that drive the AP are not compactly supported in time, they rather operate continuously. We, however, can partition them into intervals of finite duration. Then, because of the linear superposition, the overall solution of the AP will be the sum of the solutions due to individual partition elements. Each of those individual solutions has a quasi-lacuna, and once the computational domain falls completely into it (which happens after a predetermined finite interval of time), the integration does not need to be carried on any further. In other words, we replace one long-time integration of the AP by a series of short-time integrations, which allows us to limit any potentially negative effect of the ABC or PML uniformly in time.

Let us emphasize that the assumption of good performance of the original ABC or PML over a limited yet non-negligible period of time is important. If the original treatment of the outer boundary causes an immediate rapid increase of the error, then the approach proposed in this paper will not be able to correct it. For example, following the methodology of [26], it was proven in [27] that Higdon's and other similar ABCs are strongly stable in the sense that they guarantee the existence of a non-increasing energy functional. As, however, pointed out by the authors of [27] and also by Ditkowski [28], this requires sufficiently smooth data. Otherwise, Higdon's ABCs may become unstable, and then lacunae-based integration will not provide a remedy.

Note that a number of papers in the literature refer to the Huygens' principle as a useful tool for many applications, including the development of numerical methods. In most cases, however, what these publications exploit is not the full fledged Huygens' principle, but rather the well-known Huygens' construction, which is common, e.g., in optics [29]. The difference is fundamental. The Huygens' principle sets forth the existence of aft fronts of the waves and is accompanied by additional constraints, such as the odd number of space dimensions. The Huygens' construction, on the other hand, deals only with the propagating fronts; it considers the front at every given moment of time as a collection of secondary sources so that the propagating field at subsequent moments of time can be interpreted as the field due to those sources.

The Huygens' secondary sources and the Huygens' construction have proven useful, in particular, in the area of active control of sound. The JMC method (Jessel–Mangiante–Canevet), see [30–35] and also [36,37], uses the information about the noise to be canceled at the perimeter (surface) of the region to be protected, and explicitly builds the Huygens' anti-noise sources in the form of acoustic monopoles, dipoles, and quadrupoles at the boundary (see [38] for a brief comparison of JMC with other active noise control methods). A similar idea was used by Charles et al. [39] and Mangiante and Charles in [40] to build the absorbing boundary conditions for computational acoustics. Namely, the Huygens' secondary sources in [39,40] eliminate the outgoing acoustic waves in the special transition region that surrounds the computational domain.

In electromagnetism, the Huygens' construction can be interpreted as a particular realization of the electromagnetic equivalence theorem by Schelkunoff [41], see also [12, Section 8.4]. This theorem says that the field on a given region (interior or exterior), regardless of its actual sources located outside of this region, can be reproduced as the field from the specially chosen auxiliary currents at the boundary of the region. If the boundary is identified with a "frozen" propagating front at a given fixed moment of time, then the equivalence theorem yields the Huygens' construction.

In work [42,43], Bérenger uses the equivalence theorem to design the subgridding techniques for the numerical solution of Maxwell's equations; in work [44], the subgridding approach of [42,43] is extended by Costen and Bérenger to the case of frequency dependent (i.e., dispersive) media; and in work [45], Bérenger builds the Huygens' absorbing boundary conditions for time-domain Maxwell's equations. In this approach, the Huygens' secondary sources cancel out the outgoing electromagnetic field and hence prevent it from getting reflected off the artificial outer boundary. Even though there is no formal connection, work [45] can be thought of as an extension of work [39,40] from the scalar acoustic fields to the vector electromagnetic fields.

We re-emphasize though that all of the aforementioned papers exploit only the Huygens' construction for forward propagation, and never make any use of the full Huygens' principle, i.e., of the presence of aft fronts and lacunae. The latter represent a considerably more subtle phenomenon, and as mentioned by Gårding [46], can be thought of as "the result of fancy cancellations between branches of analytic functions." There are actually very few publications in the literature that do attempt to apply the ideas related to the aft fronts and lacunae in the numerical context, and among those we mention work by Warchall [47,48]. The focus of this work is on the study of domains of dependence and domains of influence for constant coefficient hyperbolic systems, and on the development of the treatment of artificial boundaries that would take advantage of the fact that the data at a given time only inside the domain fully determine the propagation through the outer boundary at all subsequent times. This work by Warchall, however, presents only preliminary theoretical observations. Its practical

implementation, if there is ever one, is contingent upon the availability of "an explicit method for propagation of waves through an artificial domain boundary, using only data at a single time inside the domain, in such a way as to duplicate exactly the propagation in unbounded space." As of yet, such a method has not been found. Contrary to that, the algorithm we present hereafter uses the right-hand sides (source terms of the governing equations), rather than the Cauchy data, to propagate the information through the artificial boundaries.

The rest of the current paper is organized as follows. In Section 2, we introduce the notion of quasi-lacunae for Maxwell's equations and describe the lacunae-based time-marching algorithm. In Section 3 we outline the idea of implementing the lacunae-based integration on its own, i.e., without having it coupled with any ABC or PML. In Section 4, we prove that for a given computational domain of finite size, lacunae-based integration guarantees that any errors related to the outer boundary will remain uniformly bounded for all times. This is our central theoretical result. It holds for any type of treatment chosen for the artificial boundary, whether it is an ABC or a PML. Moreover, the chosen treatment does not have to be modified in any way for the lacunae-based integration to apply. In Section 5, we describe the actual numerical procedure that we use; it includes the decomposition of the original problem into the interior and auxiliary sub-problems and application of the method to non-Huygens' problems. Section 6 describes the numerical setup, and Section 7 contains the results of our computations in a non-Huygens' setting, for which the three-dimensional Maxwell equations are terminated by an unsplit PML. These results corroborate the theoretical design properties of the algorithm. Section 8 contains conclusions and discussion.

2. Time-marching using quasi-lacunae of Maxwell's equations

The propagation of unsteady electromagnetic waves in vacuum is governed by the time-dependent Maxwell's equations:

$$\frac{1}{c}\frac{\partial \mathbf{E}}{\partial t} - \operatorname{curl}\mathbf{H} = -\frac{4\pi}{c}\mathbf{j}, \tag{1}$$

$$\frac{1}{c}\frac{\partial \mathbf{H}}{\partial t} + \operatorname{curl}\mathbf{E} = -\frac{4\pi}{c}\mathbf{j}^{\mathrm{M}}. \tag{2}$$

In system (1) and (2), $\mathbf{E}$ is the electric field, $\mathbf{H}$ is the magnetic field, c is the speed of light, and the normalization is chosen so that both the permittivity and permeability of vacuum are equal to one, $\varepsilon_0 = \mu_0 = 1$. Eq. (1), the Ampère law, is driven by the external electric current with the density $\mathbf{j} = \mathbf{j}(\mathbf{x},t)$, and Eq. (2), the Faraday law, is driven by the external magnetic current with the density $\mathbf{j}^{\mathrm{M}} = \mathbf{j}^{\mathrm{M}}(\mathbf{x},t)$. Eqs. (1) and (2) are supplemented by two steady-state equations, the Gauss law of electricity:

$$\operatorname{div}\mathbf{E} = 4\pi\rho, \tag{3}$$

and the Gauss law for magnetism:

$$\operatorname{div}\mathbf{H} = 4\pi\rho^{\mathrm{M}}, \tag{4}$$

where the quantities $\rho = \rho(\mathbf{x},t)$ and $\rho^{\mathrm{M}} = \rho^{\mathrm{M}}(\mathbf{x},t)$ are densities of the electric and magnetic charge, respectively. Note that whereas the electric charge ρ and current $\mathbf{j}$ have a precise physical meaning, see, e.g., [49], the magnetic charge ρ^{M} and current $\mathbf{j}^{\mathrm{M}}$ do not exist in nature and are introduced only for the convenience of mathematical analysis, as they make Eqs. (1)–(4) look symmetric.

The currents and charges that drive system (1)–(4) are subject to the conservation requirement [49,50]. For sufficiently smooth solutions, the conservation of electric charge can be written in the form of the continuity equation:

$$\frac{\partial \rho}{\partial t} + \operatorname{div}\mathbf{j} = 0. \tag{5}$$

Then, taking the divergence of both sides of Eq. (1) and using Eq. (5), we obtain:

$$\frac{\partial}{\partial t}\operatorname{div}\mathbf{E} = 4\pi\frac{\partial \rho}{\partial t}.$$

Integrating this equality from $t = 0$ to a given time t and assuming for simplicity that the initial conditions are zero, we arrive at Eq. (3). We therefore conclude that in the time-dependent framework the Gauss law of electricity shall be regarded as an implication of the Ampère law and the conservation requirement. In particular, the charge $\rho = \rho(\mathbf{x},t)$ on the right-hand side (RHS) of Eq. (3) shall be interpreted as the charge accumulated from $t = 0$ to the present moment of time t due to the current $\mathbf{j}(\mathbf{x},t)$. If $\operatorname{div}\mathbf{j} = 0$, then $\frac{\partial \rho}{\partial t} = 0$ and no accumulation of charge occurs. A similar conclusion can be drawn regarding the accumulation of magnetic charge and the Gauss law for magnetism (4).

Next, taking curl of Eq. (2), differentiating Eq. (1) with respect to time, substituting into one another, and using the identity $\operatorname{curl}\operatorname{curl}\mathbf{E} = -\Delta\mathbf{E} + \operatorname{grad}\operatorname{div}\mathbf{E}$ along with Eq. (3), we arrive at the vector d'Alembert equation for the electric field:

$$\frac{1}{c^2}\frac{\partial^2 \mathbf{E}}{\partial t^2} - \Delta\mathbf{E} = -4\pi\left[\frac{1}{c^2}\frac{\partial \mathbf{j}}{\partial t} + \frac{1}{c}\operatorname{curl}\mathbf{j}^{\mathrm{M}} + \operatorname{grad}\rho\right]. \tag{6}$$

A very similar argument yields the vector d'Alembert equation for the magnetic field:

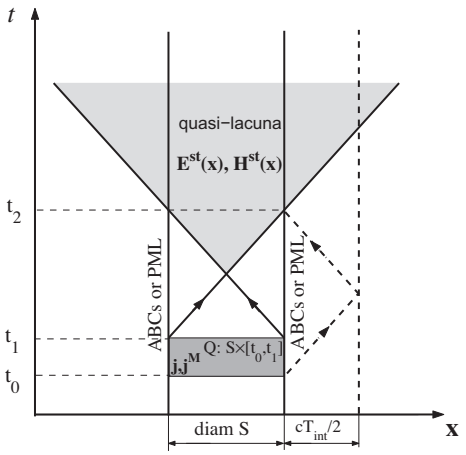

Fig. 1. Quasi-lacuna of the solution generated by compactly supported sources.

$$\frac{1}{c^2}\frac{\partial^2 \mathbf{H}}{\partial t^2} - \Delta \mathbf{H} = -4\pi\left[\frac{1}{c^2}\frac{\partial \mathbf{j}^{\mathrm{M}}}{\partial t} - \frac{1}{c}\operatorname{curl}\mathbf{j} + \operatorname{grad}\rho^{\mathrm{M}}\right]. \tag{7}$$

Let us now assume that the currents $\mathbf{j}$ and $\mathbf{j}^{\mathrm{M}}$ are compactly supported in space and time on some bounded domain $Q \subset \mathbb{R}^3 \times [0, +\infty]$. If the RHSs of Eqs. (6) and (7) were compactly supported as well, then we could have claimed that the solutions $\mathbf{E}$ and $\mathbf{H}$ have classical lacunae in the sense of Petrowsky [20]. However, due to the terms $\operatorname{grad}\rho$ and $\operatorname{grad}\rho^{\mathrm{M}}$, the RHSs of Eqs. (6) and (7) may remain non-zero even after the currents $\mathbf{j}$ and $\mathbf{j}^{\mathrm{M}}$ cease to operate. This corresponds to the accumulation of electric charge according to the continuity equation (5), and to the accumulation of magnetic charge according to the similar equation: $\frac{\partial \rho^{\mathrm{M}}}{\partial t} + \operatorname{div}\mathbf{j}^{\mathrm{M}} = 0$. Then, as we have shown in [19], instead of the classical lacunae the solutions $\mathbf{E} = \mathbf{E}(\mathbf{x}, t)$ and $\mathbf{H} = \mathbf{H}(\mathbf{x}, t)$ *will have quasi-lacunae*:

$$\mathbf{E} = \mathbf{E}^{\mathrm{st}}, \quad \mathbf{H} = \mathbf{H}^{\mathrm{st}} \quad \forall \mathbf{x}, t \in \bigcap_{(\xi,\tau)\in Q} \{(\mathbf{x}, t) \,|\, |\mathbf{x} - \boldsymbol{\xi}| < c(t - \tau), t > \tau\}. \tag{8}$$

In formula (8), $\mathbf{E}^{\mathrm{st}} = \mathbf{E}^{\mathrm{st}}(\mathbf{x})$ and $\mathbf{H}^{\mathrm{st}} = \mathbf{H}^{\mathrm{st}}(\mathbf{x})$ are the electrostatic and magnetostatic fields due to the accumulated electric and magnetic charges $\rho = \rho(\mathbf{x})$ and $\rho^{\mathrm{M}} = \rho^{\mathrm{M}}(\mathbf{x})$. These fields satisfy the Poisson equations:

$$\Delta \mathbf{E}^{\mathrm{st}} = 4\pi \operatorname{grad}\rho \tag{9}$$

and

$$\Delta \mathbf{H}^{\mathrm{st}} = 4\pi \operatorname{grad}\rho^{\mathrm{M}}, \tag{10}$$

respectively. In addition, $\mathbf{E}^{\mathrm{st}}$ and $\mathbf{H}^{\mathrm{st}}$ would have vanished if they were to extend all the way to infinity. For every moment of time t though, the fields $\mathbf{E}^{\mathrm{st}}$ and $\mathbf{H}^{\mathrm{st}}$ are defined not on the entire space $\mathbb{R}^3$, but only inside what would have been a classical lacuna of the corresponding solution,[1] i.e., behind the aft (trailing) fronts of the propagating waves. In other words, unlike in the case of classical lacunae, when the solution behind aft fronts is identically zero, in the case of quasi-lacunae the solution behind aft front reaches a steady state yet it is not necessarily zero. The existence of sharp aft fronts in odd-dimension spaces is known as the Huygens' principle, see, e.g. [51,52].

Formula (8), along with (9) and (10), can be proven by analyzing the solution in the form of the Kirchhoff integral, and showing that for the points inside the lacuna it reduces to the classical Newton's volume potential; see [19] for detail. Qualitatively, the concept of quasi-lacunae can be interpreted as a gradual onset of the electrostatic (and magnetostatic) solution. Indeed, the unsteady waves generated by the compactly supported currents $\mathbf{j}(\mathbf{x}, t)$ and $\mathbf{j}^{\mathrm{M}}(\mathbf{x}, t)$ propagate toward infinity, leaving behind their aft fronts the steady-state solution for the electromagnetic field driven by the charges $\rho(\mathbf{x})$ and $\rho^{\mathrm{M}}(\mathbf{x})$. As $t \to \infty$, the area occupied by the steady-state solution expands, and in the limit it will coincide with the entire space $\mathbb{R}^3$. Note also that if $\rho = \rho^{\mathrm{M}} = 0$, then the steady-state solution is zero as well, and the quasi-lacuna becomes a conventional lacuna. This happens, in particular, when the currents $\mathbf{j}$ and $\mathbf{j}^{\mathrm{M}}$ are solenoidal: $\operatorname{div}\mathbf{j} = 0$ and $\operatorname{div}\mathbf{j}^{\mathrm{M}} = 0$.

The existence of quasi-lacunae suggests the following way of integrating system (1) and (2). Let $S \subset \mathbb{R}^3$ be a bounded computational domain, on which the currents $\mathbf{j}$ and $\mathbf{j}^{\mathrm{M}}$ are compactly supported in space, so that on $\mathbb{R}^3 \setminus S$ the Maxwell equations are homogeneous. Moreover, let those currents operate only between the moments of time t_0 and t_1. In other words, we are assuming that the currents are compactly supported on the region $Q = \{(\mathbf{x}, t) | \mathbf{x} \in S, t_0 < t < t_1\}$ in space–time, see Fig. 1. Our

[1] The intersection of all characteristic cones (i.e., light cones) of the wave equation (6) or (7) once the vertex of the cone sweeps the support Q of the RHS.

objective is to compute the fields **E** and **H** only on S, while truncating all of its unbounded complement and replacing it by an ABC or a PML at the outer boundary ∂S.

Let us introduce the time interval T_{int} defined as the sum of the time needed for the waves to cross the domain S plus the operational time of the sources $T_0 = t_1 - t_0$:

$$T_{\text{int}} \stackrel{\text{def}}{=} \frac{1}{c}\operatorname{diam} S + T_0. \tag{11a}$$

Then, we can make the following easy observation. By the time

$$t_2 \stackrel{\text{def}}{=} t_0 + T_{\text{int}} \tag{11b}$$

the domain S will completely fall into the quasi-lacuna (8), and will remain inside the quasi-lacuna for all $t > t_2$. In other words, once the currents ceases to operate (at $t = t_1$), it takes an additional $\frac{1}{c}\operatorname{diam} S$ "seconds" for the waves they have generated to leave the domain S. Consequently, we can integrate system (1) and (2) on the finite interval T_{int} using any appropriate scheme, and then stop the integration, because at $t_2 = t_0 + T_{\text{int}}$ the solution on S reaches its steady state and remains unchanged thereafter. If we terminate the computational domain by an ABC or a PML, then no adverse phenomenon, such as an instability, related to the treatment of the outer boundary ∂S will be able to manifest itself in the course of integration, provided that the interval T_{int} is not too long.

We, however, cannot restrict ourselves to the case of external currents operating for a limited period of time only. Let us therefore consider the currents on the RHS of system (1) and (2) that operate continuously for $0 < t < +\infty$ while still being compactly supported in space on the bounded domain S. We can partition these currents into the intervals of finite duration T_0:

$$\begin{aligned}
&\mathbf{j}(\mathbf{x},t) = \sum_{i=0}^{\infty} \mathbf{j}_i(\mathbf{x},t), \quad \mathbf{j}_i(\mathbf{x},t) = \begin{cases} \mathbf{j}(\mathbf{x},t), & iT_0 \leqslant t < (i+1)T_0, \\ 0, & \text{otherwise}, \end{cases} \\
&\mathbf{j}^{\mathrm{M}}(\mathbf{x},t) = \sum_{i=0}^{\infty} \mathbf{j}_i^{\mathrm{M}}(\mathbf{x},t), \quad \mathbf{j}_i^{\mathrm{M}}(\mathbf{x},t) = \begin{cases} \mathbf{j}^{\mathrm{M}}(\mathbf{x},t), & iT_0 \leqslant t < (i+1)T_0, \\ 0, & \text{otherwise}. \end{cases}
\end{aligned} \tag{12}$$

Then, each system (1) and (2) driven by the RHS (12) for a particular i (a partial subproblem) will have a quasi-lacuna, and as such, can be integrated independently starting from

$$t_0^{(i)} \stackrel{\text{def}}{=} iT_0 \tag{13a}$$

until [cf. formula (11b)]

$$t_2^{(i)} \stackrel{\text{def}}{=} t_0^{(i)} + T_{\text{int}}, \tag{13b}$$

where T_{int} is given by (11a). At $t_2^{(i)}$, the solution to partial subproblem i reaches its steady state on the domain of interest S. Hence, it does not need to be advanced any further. The overall solution can subsequently be obtained by linear superposition. If each partial subproblem is terminated by an ABC or a PML at ∂S, then no detrimental effect related to the chosen treatment of the outer boundary will manifest itself provided that the integration interval T_{int} of (11a) is not too long.

Time-marching of the overall solution requires summation of the individual contributions for all $i = 0, 1, 2, \ldots$ However, the causality principle implies that for any given moment of time t, no portion of the RHS (12) that corresponds to later times can contribute to the solution. Therefore, the summation will not extend to infinity and will rather terminate at $N_1 \stackrel{\text{def}}{=} \lceil t/T_0 \rceil - 1$, where $\lceil\cdot\rceil$ is the ceiling function, i.e., the smallest integer greater than or equal to its argument. Otherwise, there will be terms of two different types in the sum. First, there will be a finite number of unsteady terms $\mathbf{E}_i(\mathbf{x},t)$ and $\mathbf{H}_i(\mathbf{x},t)$, $i = N_0, \ldots, N_1$, [solutions of (1) and (2), (12)] that have not reached their steady state on S yet, and still need to be taken into account. The index N_0 corresponds to the last term, counting backwards, for which the domain S is not completely inside the quasi-lacuna yet; it is given by $N_0 = \left\lfloor \frac{t - \operatorname{diam} S/c}{T_0} \right\rfloor$, where $\lfloor\cdot\rfloor$ denotes integer part. In addition, there will be steady-state terms in the overall sum for each field: $\mathbf{E}^{\text{st}}_{N_0}(\mathbf{x})$ and $\mathbf{H}^{\text{st}}_{N_0}(\mathbf{x})$. These terms are generated by the electric and magnetic charges, respectively, accumulated over the period $0 < t < N_0 T_0$, i.e., for the operational time of the first N_0 partial sources (12), $i = 0, \ldots, N_0 - 1$. Altogether, we can thus write:

$$\mathbf{E}(\mathbf{x},t) = \mathbf{E}^{\text{st}}_{N_0}(\mathbf{x}) + \sum_{i=N_0}^{N_1} \mathbf{E}_i(\mathbf{x},t), \tag{14}$$

and a similar expression for the magnetic field. It is very important that the number of unsteady terms on the RHS of Eq. (14) remains bounded for all times and $N_1 - N_0 + 1 \leqslant \left\lceil \frac{\operatorname{diam} S/c}{T_0} \right\rceil + 2$.

The fields $\mathbf{E}^{\text{st}}_{N_0}(\mathbf{x})$ and $\mathbf{H}^{\text{st}}_{N_0}(\mathbf{x})$ are the electrostatic and magnetostatic contributions, respectively, to the total electromagnetic field. They are due to the external charges that are given functions of space and time. In formula (14) and the similar expression for $\mathbf{H}(\mathbf{x},t)$, these static fields are to be evaluated at the time $t = N_0 T_0$. This can be done by solving the Poisson

equations (9) and (10) on S, subject to the appropriate (Laplace) ABC at the boundary ∂S. Interpretation of $\mathbf{E}^{\mathrm{st}}_{N_0}(\mathbf{x})$ and $\mathbf{H}^{\mathrm{st}}_{N_0}(\mathbf{x})$ as solutions of the Poisson equation on S is useful for the theoretical analysis that leads to Theorem 1, see the discussion on p. 12.

In practice, however, $\mathbf{E}^{\mathrm{st}}_{N_0}(\mathbf{x})$ and $\mathbf{H}^{\mathrm{st}}_{N_0}(\mathbf{x})$ can be obtained without having to actually solve Eqs. (9) and (10). Instead, those fields can be computed on S in the course of regular time-marching once the unsteady part of the solution has left the domain, see Section 6.8.

Let us reiterate that if $\mathrm{div}\mathbf{j} = 0$ and $\mathrm{div}\mathbf{j}^{\mathrm{M}} = 0$, then neither the electric nor magnetic charge accumulates because $\frac{\partial \rho}{\partial t} = 0$ and $\frac{\partial \rho^{\mathrm{M}}}{\partial t} = 0$, and the quasi-lacuna transforms into a conventional lacuna. The field inside the conventional lacuna is zero, and accordingly, there is no steady-state contribution $\mathbf{E}^{\mathrm{st}}_{N_0}(\mathbf{x})$ to the sum (14) in this case (likewise for the magnetic field). In our previous work [24,25], we have built a family of numerical algorithms for Maxwell's equations that relied on conventional lacunae. In particular, the algorithm of [25] offered stabilization of PMLs. Those algorithms, however, required construction of the special solenoidal auxiliary currents, which was accomplished theoretically, but in practice led to additional overheads.*The key advantage of using quasi-lacunae instead of classical lacunae for time-marching the Maxwell's equations is that they impose no constraints on the sources of the field.* This is due to the steady-state term in the sum (14) that carries forward the "residual" contribution of all those partial sources (12), for which the unsteady waves have already left the domain S. Yet another advantage compared to work [25] is that in the current paper we show how *quasi-lacunae can help stabilize the treatment of outer boundaries for general non-Huygens' problems.*

3. Standalone implementation

Besides having it coupled with an ABC or a PML, lacunae-based integration can be implemented on its own. This, in fact, was the original approach, see [21,22]. During the time interval T_{int} the maximum distance any wave can travel in space is cT_{int}. Therefore, we can consider external boundaries with arbitrary (reflecting) properties for solving each of the individual Maxwell's systems for $i = 0, 1, 2, \ldots$ As long as none of these boundaries is located closer than half of that maxim distance, $c\,T_{\mathrm{int}}/2$, to ∂S, the solution $\mathbf{E}_i$, $\mathbf{H}_i$ inside S will not feel their presence for $t_0^{(i)} \leqslant t \leqslant t_2^{(i)}$. In other words, to obtain the correct solution on the domain of interest S, each individual solution $\mathbf{E}_i$, $\mathbf{H}_i$ needs to be computed on a bounded auxiliary domain of the maximum size $Z = \mathrm{diam}\,S + c\,T_{\mathrm{int}}$, see Fig. 1. Compared to setting an ABC or a PML at ∂S, this approach requires a larger computational domain, *yet appears provably free from any error associated with the grid truncation.*

In [21,22], the standalone lacunae-based integration was successfully applied to the scalar d'Alembert equation; in [23] the methodology was extended to the equations of acoustics, and [24] it was extended further — to Maxwell's equations. Moreover, in the recent paper [53] lacunae-based open boundary conditions have been constructed and tested for a considerably more general setting than linear wave-type equations — 2D nonlinear dissipative magnetohydrodynamics (MHD). Even in this context, when the existence of lacunae can be claimed only approximately rather than exactly, lacunae-based ABCs have consistently outperformed other more standard ABCs.

4. A temporally uniform error bound

In this section, we show that time-marching Maxwell's equations with the help of quasi-lacunae, as suggested in Sections 2 and 3, eliminates all possible error growth that may originate from setting an ABC or a PML at the boundary ∂S of the computational domain S.

In matrix notation, Maxwell's equations (1) and (2), along with the appropriate initial conditions, can be written as

$$\begin{aligned} &\frac{1}{c}\frac{\partial \mathbf{w}}{\partial t} + \widehat{\mathbf{L}}\mathbf{w} = \mathbf{f}(\mathbf{x},t), \quad \mathbf{x}\in\mathbb{R}^3,\ t>0,\\ &\mathbf{w}(\mathbf{x},0) = \boldsymbol{\varphi}(\mathbf{x}), \quad \mathbf{x}\in\mathbb{R}^3, \end{aligned} \tag{15}$$

where $\mathbf{w} = [\mathbf{E},\mathbf{H}]^T$ is the vector of field components, $\widehat{\mathbf{L}}$ is the operator written as a symbolic matrix:

$$\widehat{\mathbf{L}} = \begin{bmatrix} 0 & -\mathrm{curl} \\ \mathrm{curl} & 0 \end{bmatrix}, \tag{16}$$

$\boldsymbol{\varphi}(\mathbf{x})$ is the initial data, and $\mathbf{f}(\mathbf{x},t) = [-4\pi\mathbf{j}(\mathbf{x},t)/c, -4\pi\mathbf{j}^{\mathrm{M}}(\mathbf{x},t)/c]^T$ is the RHS of the Maxwell system. Both $\boldsymbol{\varphi}(\mathbf{x})$ and $\mathbf{f}(\mathbf{x},t)$ are assumed compactly supported in space, so that the far field part of problem (15) is homogeneous. To solve problem (15) on the computer, we choose a bounded computational domain S such that $\mathrm{supp}\,\boldsymbol{\varphi} \subset S$ and $\mathrm{supp}\,\mathbf{f} \subset S$, and set an ABC or a PML at its boundary ∂S:

$$\begin{aligned} &\frac{1}{c}\frac{\partial \mathbf{w}^{(S)}}{\partial t} + \widehat{\mathbf{L}}\mathbf{w}^{(S)} = \mathbf{f}(\mathbf{x},t), \quad \mathbf{x}\in S, \quad t>0,\\ &\widehat{\boldsymbol{\Gamma}}\mathbf{w}^{(S)}(\mathbf{x},t) = \mathbf{0}, \quad \mathbf{x}\in\partial S, \quad t>0,\\ &\mathbf{w}^{(S)}(\mathbf{x},0) = \boldsymbol{\varphi}(\mathbf{x}), \quad \mathbf{x}\in S. \end{aligned} \tag{17}$$

The operator $\widehat{\boldsymbol{\Gamma}}$ in formula (17) represents the aforementioned ABC or PML. In the case of an ABC, $\widehat{\boldsymbol{\Gamma}}$ specifies certain (local) relations between the field components and, perhaps, their derivatives. In the case of a PML, the operator $\widehat{\boldsymbol{\Gamma}}$ does not have a

straightforward explicit definition. Having such a definition though is not even necessary for the purpose of our analysis. It is sufficient to assume that the relations between the field components $\mathbf{w}^{(S)}(\mathbf{x},t)$ enforced by $\widehat{\mathbf{\Gamma}}$ are equivalent to setting a specific PML outside ∂S.

An ideal ABC or PML would guarantee that the solutions of problems (15) and (17) coincide on the domain S

$$\mathbf{w}(\mathbf{x},t) \equiv \mathbf{w}^{(S)}(\mathbf{x},t), \quad \mathbf{x} \in S, \tag{18}$$

for any moment of time $t > 0$. In practice, however, this can hardly be achieved, and instead of equality (18) we would normally expect that the following inequality holds:

$$\|\mathbf{w}(\mathbf{x},t) - \mathbf{w}^{(S)}(\mathbf{x},t)\| \leqslant \delta(\widehat{\mathbf{\Gamma}}), \quad \mathbf{x} \in S. \tag{19}$$

The constant δ on the RHS of (19) depends on the operator $\widehat{\mathbf{\Gamma}}$, i.e., on the quality of the ABC or PML at ∂S. In the ideal case, $\delta = 0$, and then (19) transforms into (18). Otherwise, δ is non-zero; in the case of an ABC it may depend, for example, on the order of the boundary condition (see,e.g., [54–56]), whereas in the case of a PML it may depend, in particular, on its thickness. In all cases, however, a non-deteriorating long-time performance implies that δ does not depend on time, or more precisely, remains bounded as the time elapses.

As mentioned in Section 1 though, this is not always the case either. To account for the possible adverse behavior, we follow the suggestion of [10] and interpret any long-time error growth as the growth of small perturbations in the data that drive the problem.[2] Specifically, along with the true bounded-domain solution $\mathbf{w}^{(S)}$ that satisfies system (17), we consider its perturbed counterpart $\tilde{\mathbf{w}}^{(S)}$ that satisfies the system with the perturbed boundary data, initial data, and the RHS:

$$\begin{aligned}
&\frac{1}{c}\frac{\partial \tilde{\mathbf{w}}^{(S)}}{\partial t} + \widehat{\mathbf{L}}\tilde{\mathbf{w}}^{(S)} = \mathbf{f}(\mathbf{x},t) + \boldsymbol{\mu}, \quad \mathbf{x} \in S,\ t > 0,\\
&\widehat{\mathbf{\Gamma}}\tilde{\mathbf{w}}^{(S)}(\mathbf{x},t) = \boldsymbol{\epsilon}, \quad \mathbf{x} \in \partial S, \quad t > 0,\\
&\tilde{\mathbf{w}}^{(S)}(\mathbf{x},0) = \boldsymbol{\varphi}(\mathbf{x}) + \boldsymbol{\xi}, \quad \mathbf{x} \in S.
\end{aligned} \tag{20}$$

The difference between the perturbed and unperturbed solutions may grow on the domain S as the time t elapses:

$$\|\tilde{\mathbf{w}}^{(S)}(\mathbf{x},t) - \mathbf{w}^{(S)}(\mathbf{x},t)\| \leqslant \eta(t)\|[\boldsymbol{\mu}, \boldsymbol{\epsilon}, \boldsymbol{\xi}]\|'. \tag{21}$$

The rate of growth $\eta(t)$ is determined by a particular ABC or PML; for example, some well-known PMLs have been reported to demonstrate a linear or quadratic growth [8,57,10]. The notation $[\boldsymbol{\mu}, \boldsymbol{\epsilon}, \boldsymbol{\xi}]$ on the RHS of inequality (21) represents a symbolic vector of all perturbations of the data in system (20). The choice of norms $\|\cdot\|$ and $\|\cdot\|'$ for some specific cases is discussed in [8,57,10].

We emphasize that inequality (21) is quite general in the sense that it allows the perturbations of the data to grow with a prescribed rate, yet the reason for the growth may be arbitrary and it does not need to be known.

Inequality (21) implies that the perturbations that are small initially may increase with no bound for large integration times. If, however, the plain integration of system (17) is replaced by the integration that uses quasi-lacunae (see Section 2), then estimate (21) can be drastically improved and, in fact, made *uniform in time*. Indeed, both solutions, $\mathbf{w}^{(S)}(\mathbf{x},t)$ and $\tilde{\mathbf{w}}^{(S)}(\mathbf{x},t)$, can be partitioned similarly to how it is done in Eq. (14):

$$\mathbf{w}^{(S)}(\mathbf{x},t) = \mathbf{w}_{N_0}^{(S),\mathrm{st}}(\mathbf{x}) + \sum_{i=N_0}^{N_1} \mathbf{w}_i^{(S)}(\mathbf{x},t), \tag{22}$$

$$\tilde{\mathbf{w}}^{(S)}(\mathbf{x},t) = \tilde{\mathbf{w}}_{N_0}^{(S),\mathrm{st}}(\mathbf{x}) + \sum_{i=N_0}^{N_1} \tilde{\mathbf{w}}_i^{(S)}(\mathbf{x},t), \tag{23}$$

where $\mathbf{w}_{N_0}^{(S),\mathrm{st}}(\mathbf{x})$, $\tilde{\mathbf{w}}_{N_0}^{(S),\mathrm{st}}(\mathbf{x})$ and $\mathbf{w}_i^{(S)}(\mathbf{x},t)$, $\tilde{\mathbf{w}}_i^{(S)}(\mathbf{x},t)$, $i = N_0,\ldots,N_1$, represent the corresponding steady-state and time-dependent terms, respectively. Since each unsteady term needs to be integrated only for a limited time T_{int}, see formula (11a), estimate (21) yields for $i = N_0,\ldots,N_1$:

$$\left\|\tilde{\mathbf{w}}_i^{(S)}(\mathbf{x},t) - \mathbf{w}_i^{(S)}(\mathbf{x},t)\right\| \leqslant C_0\|[\boldsymbol{\mu}_i, \boldsymbol{\epsilon}_i, \boldsymbol{\xi}_i]\|', \tag{24}$$

where $C_0 = \eta(T_{\mathrm{int}})$ is a constant, and $[\boldsymbol{\mu}_i, \boldsymbol{\epsilon}_i, \boldsymbol{\xi}_i]$ are the perturbations of the data for the ith partial problem. As the overall number of unsteady terms $N_1 - N_0 + 1$ in either sum (22) or (23) does not exceed the value $\left[\frac{\mathrm{diam}\, S/c}{T_0}\right] + 2$ for all times, we can use the triangle inequality and obtain the following estimate for the unsteady contributions to the sums (22) and (23):

$$\left\|\sum_{i=N_0}^{N_1} \tilde{\mathbf{w}}_i^{(S)}(\mathbf{x},t) - \sum_{i=N_0}^{N_1} \mathbf{w}_i^{(S)}(\mathbf{x},t)\right\| \leqslant C_1 \sup_i \|[\boldsymbol{\mu}_i, \boldsymbol{\epsilon}_i, \boldsymbol{\xi}_i]\|'. \tag{25}$$

[2] These perturbations may have arbitrary nature, although in the numerical context it is convenient to associate them with the residual terms of the approximation, i.e., with the truncation error.

In formula (25), $C_1 = C_0 \cdot \max\{N_1 - N_0 + 1\}$, and the supremum (least upper bound) on the RHS of the inequality can naturally be assumed bounded. We use $\max\{N_1 - N_0 + 1\}$ in the estimate because both N_1 and N_0 depend on t (see Section 2) and hence the quantity $N_1 - N_0 + 1$ is not necessarily constant; however, this quantity remains bounded for all t.

The steady-state part of the solution, $\mathbf{w}_{N_0}^{(S),\mathrm{st}}(\mathbf{x})$, may also suffer from the grid truncation effects. Indeed, the static fields $\mathbf{E}_{N_0}^{\mathrm{st}}(\mathbf{x})$ and $\mathbf{H}_{N_0}^{\mathrm{st}}(\mathbf{x})$, see formula (14), satisfy the Poisson equations (9) and (10), respectively, at $t = N_0 T_0$. Once the unbounded domain $\mathbb{R}^n$ of these equations is truncated and reduced to S, the actual steady-state component of the solution may get perturbed due to the perturbations $\boldsymbol{\psi}$ of the data, i.e., of the RHS to the Poisson equation (9) or (10), as well as of the ABC chosen to solve these equations (a steady-state ABC must still guarantee estimate (19)). Then, the difference between the perturbed and unperturbed steady-state solutions satisfies

$$\left\| \tilde{\mathbf{w}}_{N_0}^{(S),\mathrm{st}}(\mathbf{x}) - \mathbf{w}_{N_0}^{(S),\mathrm{st}}(\mathbf{x}) \right\| \leqslant C_2 \|\boldsymbol{\psi}\|'', \tag{26}$$

where C_2 is a constant. The most important consideration regarding the steady-state contribution to the overall solution though is that it needs to be evaluated at the predetermined moments of time: $t = iT_0$, $i = 1, 2, \ldots$, (see Section 2), and every time the new steady-state component is included, the previous one should be disregarded. Consequently, as long as the quantities ρ and ρ^{M} on the RHS of Eqs. (9) and (10) are given, there is no cumulative effect for the error.[3]

Finally, combining estimates (19), (25), and (26) with the help of the triangle inequality, we arrive at the following result.

Theorem 1. *Let $S \subset \mathbb{R}^3$ be a bounded computational domain, and let problem (15) be solved on S using an appropriate ABC or PML that reduces it to problem (17). Let problem (17) be time marched with the help of quasi-lacunae. Then, assuming that $\sup_i \|[\mu_i, \boldsymbol{\epsilon}_i, \xi_i]\|' < \infty$ and $\|\psi\|'' < \infty$, the error on the computational domain S will remain uniformly bounded for all times:*

$$\|\tilde{\mathbf{w}}^{(S)}(\mathbf{x}, t) - \mathbf{w}(\mathbf{x}, t)\| \leqslant \delta(\widehat{\mathbf{\Gamma}}) + C_1 \sup_i \|[\boldsymbol{\mu}_i, \boldsymbol{\epsilon}_i, \boldsymbol{\xi}_i]\|' + C_2 \|\boldsymbol{\psi}\|''. \tag{27}$$

Theorem 1 guarantees that regardless of what causes the original long-time deterioration, time-marching with the help of quasi-lacunae will prevent any possible error growth.

5. Application to non-Huygens' problems

From the standpoint of applications though, the key problem of interest is typically more sophisticated than that studied in Sections 2 and 4. It may involve some complex phenomena that take place on a bounded region $S \subset \mathbb{R}^3$, i.e., in the near field, and manifest themselves by the radiation of electromagnetic waves in the far field, i.e., in $\mathbb{R}^3 \setminus S$:

$$\begin{aligned} &\widehat{\mathbf{F}}\left(\mathbf{x}, t, \mathbf{w}, \frac{\partial \mathbf{w}}{\partial t}, \frac{\partial \mathbf{w}}{\partial \mathbf{x}}, \ldots\right) = \mathbf{0}, \quad \mathbf{x} \in S, \ t > 0, \\ &\frac{1}{c}\frac{\partial \mathbf{w}}{\partial t} + \widehat{\mathbf{L}}\mathbf{w} = \mathbf{0}, \quad \mathbf{x} \in \mathbb{R}^3 \setminus S, \ t > 0, \\ &\mathbf{w}(\mathbf{x}, 0) = \mathbf{0}, \quad \mathbf{x} \in \mathbb{R}^3 \setminus S. \end{aligned} \tag{28}$$

In formula (28), we use the generic operator notation $\widehat{\mathbf{F}}(\cdots)$ to account for everything that may potentially be going on inside S, for example, the generation of electromagnetic field by currents, scattering off specific geometric shapes, propagation though a lossy and/or dispersive medium, nonlinear effects, etc. At the same time, the far-field solution is supposed to be governed by the constant coefficient homogeneous Maxwell equations, so that the operator $\widehat{\mathbf{L}}$ in (28) is given by formula (16). The overall problem (28) is assumed uniquely solvable and well-posed.

For the purpose of solving problem (28) on the computer, the far field is, again, truncated and replaced by an ABC or a PML at the outer boundary ∂S. The goal of our study is the same as before, namely, to make sure that numerical performance of the chosen ABC or PML does not deteriorate over long time intervals. However, the method developed and analyzed in Sections 2 and 4 will not, generally speaking, apply directly to the new formulation (28). In fact, all we require of this new formulation is the overall existence, uniqueness, and well-posedness. In doing so, the near field may be quite complex, the governing equations $\widehat{\mathbf{F}}(\cdots) = \mathbf{0}$ on S may not even be Maxwell's (unlike in Sections 2 and 4), and hence the problem may not even be Huygens'. Therefore, the application of time-marching based on quasi-lacunae will require additional constructs.

Specifically, we decompose problem (28) into the interior and auxiliary problems (AP). This decomposition was introduced previously for the integration techniques and the ABCs based on conventional lacunae, see [21–24]. The interior problem is posed on S:

$$\begin{aligned} &\widehat{\mathbf{F}}\left(\mathbf{x}, t, \mathbf{w}, \frac{\partial \mathbf{w}}{\partial t}, \frac{\partial \mathbf{w}}{\partial \mathbf{x}}, \ldots\right) = \mathbf{0}, \quad \mathbf{x} \in S, \ t > 0, \\ &\mathbf{w}(\mathbf{x}, t) = \mathbf{w}^{\mathrm{aux}}(\mathbf{x}, t), \quad \mathbf{x} \in \partial S, \ t > 0, \end{aligned} \tag{29}$$

[3] In the current version of the algorithm, we do not solve the Poisson equations (9) and (10) explicitly, and rather use the steady-state solution that forms inside the quasi-lacunae in the course of time-marching. The resulting effect on the accumulation of error is discussed on page 23, around Eq. (61).

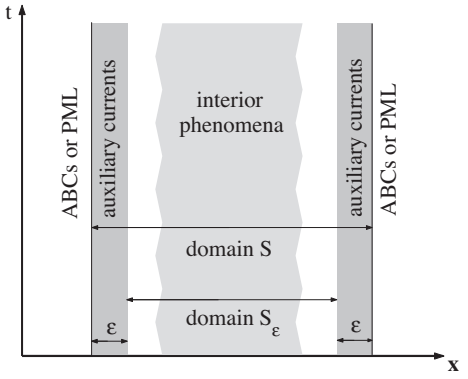

Fig. 2. Computational setup for a non-Huygens' problem.

and instead of an ABC (or a PML) at the outer boundary, we simply require that its solution coincide at ∂S with the solution $\mathbf{w}^{\text{aux}}(\mathbf{x},t)$ of the AP. The AP, in turn, is formulated on the entire space $\mathbb{R}^3$ as a pure Maxwell's system in vacuum subject to the homogeneous initial conditions:

$$\begin{aligned} &\frac{1}{c}\frac{\partial \mathbf{w}^{\text{aux}}}{\partial t}+\widehat{\mathbf{L}}\mathbf{w}^{\text{aux}}=\mathbf{f}^{\text{aux}}(\mathbf{x},t), \quad \mathbf{x}\in\mathbb{R}^3,\ t>0,\\ &\mathbf{w}^{\text{aux}}(\mathbf{x},0)=\mathbf{0}, \quad \mathbf{x}\in\mathbb{R}^3. \end{aligned} \tag{30}$$

Its solution is driven by the auxiliary electric and magnetic currents $\mathbf{f}^{\text{aux}}(\mathbf{x},t)=-\frac{4\pi}{c}[\mathbf{j},\mathbf{j}^{\text{M}}]^T$ that link the interior and the auxiliary problems and are constructed as follows.

Let $\mathbf{w}(\mathbf{x},t)$ be the solution to problem (28). Consider a smooth scalar function $\mu(\mathbf{x})$, which satisfies $\mu(\mathbf{x})\equiv 1$ for $\mathbf{x}\in\mathbb{R}^3\setminus S$ and $\mu(\mathbf{x})\equiv 0$ for $\mathbf{x}\in S_\varepsilon$, where $S_\varepsilon=\{\mathbf{x}|\mathbf{x}\in S,\ \text{dist}\,(\mathbf{x},\partial S)>\varepsilon\}$. In other words, $\mu(\mathbf{x})$ is zero "well inside" S, and is equal to one everywhere outside S. It undergoes a smooth transition from zero to one in a narrow region of width ε next to the boundary ∂S from the interior side, see Fig. 2.

Next, we multiply $\mathbf{w}(\mathbf{x},t)$ by $\mu(\mathbf{x})$ and apply the full left-hand side operator of Maxwell's system (15) to this product everywhere on $\mathbb{R}^3$ for all $t>0$. This yields the RHS to the AP (30):

$$\mathbf{f}^{\text{aux}}(\mathbf{x},t)\overset{\text{def}}{=}\frac{1}{c}\frac{\partial \mu\mathbf{w}}{\partial t}+\widehat{\mathbf{L}}\mu\mathbf{w}. \tag{31}$$

Obviously, $\mathbf{f}^{\text{aux}}=\mathbf{0}$ for $\mathbf{x}\in S_\varepsilon$ and any $t>0$, because $\mu=0$ on S_ε, and also $\mathbf{f}^{\text{aux}}=\mathbf{0}$ for $\mathbf{x}\in\mathbb{R}^3\setminus S$ and any $t>0$, because $\mu=1$ on $\mathbb{R}^3\setminus S$ and consequently, the function $\mu\mathbf{w}$ solves the homogeneous Maxwell equations. The only region where $\mathbf{f}^{\text{aux}}$ may differ from zero is the transition region $S\setminus S_\varepsilon$.

As the Cauchy problem for constant coefficient Maxwell's equations has a unique solution, we conclude that the solution $\mathbf{w}^{\text{aux}}(\mathbf{x},t)$ to the AP (30) driven by the auxiliary currents $\mathbf{f}^{\text{aux}}$ of (31) coincides with the solution to problem (28) everywhere on the exterior domain $\mathbb{R}^3\setminus S$ for all $t>0$.[4] Therefore, we can use this solution $\mathbf{w}^{\text{aux}}$ to supply the required outer boundary data to the interior problem (29), and thus expect that the solution $\mathbf{w}(\mathbf{x},t)$ to the latter will coincide with the solution of the original problem (28) on the interior domain S for all $t>0$.

Consequently, the solution $\mathbf{w}(\mathbf{x},t)$ needed on S for defining the auxiliary currents by means of formula (31) can be interpreted as a solution to the interior problem (29) rather than that to the original problem (28). This consideration completes the decomposition of the overall problem (28) into the interior and auxiliary sub-problems (29) and (30). The latter two problems are not independent. Solution to the AP (30) provides the boundary closure for the interior problem (29), whereas solution to the interior problem is used for generating the source terms (31) for the AP.

The AP (30) is still formulated on an unbounded region. Hence, in practice it has to be truncated and solved with the help of an ABC or a PML. It is natural to solve the AP on the same bounded domain S, see Fig. 2, and terminate it with the same ABC or PML at ∂S that we would have used for the original problem (28). In other words, *having performed the decomposition of problem (28) into problems (29) and (30), we can transfer the task of setting the ABC or PML at ∂S from the original problem (28) to the AP (30). The key benefit from employing the foregoing decomposition is that the AP satisfies the (generalized) Huygens' principle.* Therefore, we can integrate the AP using quasi-lacunae and thus guarantee the non-deteriorating performance of any ABC or PML chosen for truncating the auxiliary grid.

[4] In the literature on electromagnetism, a very similar result is often referred to as the electromagnetic equivalence theorem, see [41] or [12, Section 8.4]. It says that the field on a given region, regardless of its actual sources (outside of this region), can be reproduced as the field from the specially chosen auxiliary currents at the boundary.

At the discrete level, the interior problem and the AP are time marched synchronously. Once the interior solution is advanced by one time step, the auxiliary sources $\mathbf{f}^{\text{aux}}$ can also be advanced by one time step. Then, the exterior solution $\mathbf{w}^{\text{aux}}$ can be obtained on the next time level; it needs to be known only right outside S. This solution provides the missing closure for the interior problem on the upper time level, after which the interior solution can be advanced yet once again, and the procedure cyclically repeats itself. In Section 6, we provide the full implementation detail.

6. Numerical setup

We will implement the algorithm of Section 5 in a full 3D Cartesian setting for the computational domain shaped as a parallelepiped. At the outer surface of the parallelepiped the grid will be terminated by the unsplit PML by Zhao and Cangellaris [58], see Appendix A. This combination of the geometry and the treatment of the outer boundary is popular for CEM applications.

We will first demonstrate that the standard non-modified PML set as a wave absorber at the outer boundaries of the 3D Cartesian grid generates instabilities already at the moderate computational times. Then, we will show that the integration based on quasi-lacunae completely removes the deterioration and allows one to compute the solution for as long as required.

In the interior of the computational domain we will be solving the standard Maxwell equations in vacuum driven by the given external currents. These equations have a simple axially symmetric exact solution (a regularized oscillating dipole) that we will use as a reference for comparison with the numerical results. Let us emphasize that despite of its axial symmetry the problem will be solved using 3D Cartesian coordinates, taking no advantage of the more convenient spherical or cylindrical geometry (that could lead to a reduced dimension). This will allow us to identify the instability induced by the Cartesian PML and to demonstrate that it can be cured with a quasi-lacunae based approach. *We also re-emphasize that even though the interior problem we have currently chosen is merely the constant coefficient Maxwell equations driven by known currents, we will take no advantage of this fact and rather develop a full-fledged decomposition approach described in Section 5 that allows to treat the interior problem as non-Huygens'.*

6.1. Governing equations and geometry

Let z be the axis of symmetry for the solution. In this case, the full Maxwell system of equations gets split into two independent subsystems that correspond to the transverse magnetic (TM) and transverse electric (TE) modes. Hereafter, we focus on the TM mode. In the spherical coordinate system (r,θ,φ), the TM mode relates two non-zero components of the electric field, E_r and E_θ, and one (angular) component of magnetic field, H_φ. However, the split takes place only in the spherical or cylindrical coordinates. In the Cartesian coordinates (x,y,z), the TM mode contains a total of five Cartesian components of the field vectors E_x, E_y, E_z, H_x, and H_y (note that $H_z\equiv 0$) that satisfy the conventional Maxwell equations:

$$-\frac{\partial H_y}{\partial z}=\frac{1}{c}\frac{\partial E_x}{\partial t}+\frac{4\pi}{c}j_x, \tag{32}$$

$$\frac{\partial H_x}{\partial z}=\frac{1}{c}\frac{\partial E_y}{\partial t}+\frac{4\pi}{c}j_y, \tag{33}$$

$$\frac{\partial H_y}{\partial x}-\frac{\partial H_x}{\partial y}=\frac{1}{c}\frac{\partial E_z}{\partial t}+\frac{4\pi}{c}j_z, \tag{34}$$

$$\frac{\partial E_z}{\partial y}-\frac{\partial E_y}{\partial z}=-\frac{1}{c}\frac{\partial H_x}{\partial t}, \tag{35}$$

$$\frac{\partial E_x}{\partial z}-\frac{\partial E_z}{\partial x}=-\frac{1}{c}\frac{\partial H_y}{\partial t}, \tag{36}$$

$$\frac{\partial E_y}{\partial x}-\frac{\partial E_x}{\partial y}=0. \tag{37}$$

In this system, Eqs. (32)–(34) represent the Ampère law and are driven by the external currents j_x,j_y,j_z. The Faraday law is given by equations (35)–(37) and is homogeneous (no magnetic currents exist in nature). Eq. (37) is what remains of the Faraday's law in the z direction ($H_z\equiv 0$); it will not be a part of the numerical algorithm or subsequent analysis.

Let us now define the computational domain S. First of all, the foregoing axial symmetry implies that it is sufficient to compute the solution only within one octant, i.e., on one eighth of a Cartesian cube centered at the origin. This is because each component of the solution possesses a certain parity, i.e., E_x, E_y, E_z, H_x, and H_y are even or odd functions of the Cartesian variables x, y, and z (see Section 6.5):

$$E_x(-x)=-E_x(x),\quad E_x(-y)=E_x(y),\quad E_x(-z)=-E_x(z), \tag{38}$$

$$E_y(-x)=E_y(x),\quad E_y(-y)=-E_y(y),\quad E_y(-z)=-E_y(z), \tag{39}$$

$$E_z(-x)=E_z(x),\quad E_z(-y)=E_z(y),\quad E_z(-z)=E_z(z), \tag{40}$$

$$H_x(-x)=-H_x(x),\quad H_x(-y)=-H_x(y),\quad H_x(-z)=H_x(z), \tag{41}$$

$$H_y(-x)=-H_y(x),\quad H_y(-y)=H_y(y),\quad H_y(-z)=H_y(z). \tag{42}$$

Hence, one can compute the fields only for $x \geqslant 0$, $y \geqslant 0$, and $z \geqslant 0$. In doing so, symmetry relations (38)–(42) will provide the boundary conditions on the planes $x = 0$, $y = 0$, $z = 0$. Therefore, we choose the computational domain S in the form of a parallelepiped (see Fig. 3):

$$S = \{(x, y, z) : \ 0 \leqslant x \leqslant a, \ 0 \leqslant y \leqslant b, \ 0 \leqslant z \leqslant c\}.$$

In our experiments, we always set $a = b = c = 2.4$ cm. Electric currents j_x, j_y, and j_z that drive the solution, see equations (32)–(37), are compactly supported inside the computational domain S.

The boundary data at the outer planes $x = a$, $y = a$, and $z = a$ will be taken from the solution to the AP (auxiliary problem), in accordance with the algorithm described in Section 5.

6.2. Auxiliary problem

The AP is governed by the Maxwell equations for vacuum with the specially designed right-hand sides (auxiliary currents). The equations are essentially the same as (32)–(37) except that (i) there may be a non-physical magnetic current in the AP, and (ii) the AP is terminated by the PML that leads to a modification of the governing equations near the exterior boundaries, see Section 6.3 and Appendix A. As explained in Section 5, the AP plays a pivotal role for the analysis of non-Huygens' formulations, because the decomposition of the original problem into the interior and auxiliary problems leaves all the complex phenomena in the interior, whereas the AP itself becomes Huygens' and can therefore be treated with the help of quasi-lacunae.

The auxiliary currents are built from the solution $\mathbf{E}$, $\mathbf{H}$ to the interior problem. For example, the x-component of the electric current and the y-component of the magnetic currents are given by

$$\frac{4\pi}{c} j_x = -\frac{1}{c}\frac{\partial \mu E_x}{\partial t} - \frac{\partial \mu H_y}{\partial z}, \quad \frac{4\pi}{c} j_y^{\mathrm{M}} = \frac{1}{c}\frac{\partial \mu H_y}{\partial t} + \frac{\partial \mu E_x}{\partial z} - \frac{\partial \mu E_z}{\partial x}, \tag{43}$$

where $\mu = \mu(\mathbf{x})$ is the multiplier function introduced in Section 5. Note that since $H_z \equiv 0$ and Eq. (37) holds, the z-component of the magnetic current vanishes, $j_z^{\mathrm{M}} \equiv 0$.

Compared to the interior problem, the AP will be solved on a somewhat larger cube

$$S^{\mathrm{aux}} = \{(x, y, z) : \ 0 \leqslant x \leqslant a', \ 0 \leqslant y \leqslant a', \ 0 \leqslant z \leqslant a'\}, \tag{44}$$

where $a' > a$. The auxiliary domain S^{aux} contains the computational domain S for the interior problem, as well as the PML that extends from ∂S outward (see Fig. 3).

Next, we actually define the function $\mu(\mathbf{x})$ that specifies the shape of the transition zone where the auxiliary currents exist, and actually helps construct those auxiliary currents, see formula (43). It is convenient to choose a spherically symmetric function $\mu = \mu(r), \ r = \sqrt{x^2 + y^2 + z^2}$:

$$\mu(r) = P_4\left(\frac{r - a + \varepsilon}{\varepsilon}\right), \tag{45}$$

where $P_4(x)$ is smooth, equal to zero for $x \leqslant 0$, equal to one for $x \geqslant 1$, and coincides with a polynomial of degree seven on the interval $0 \leqslant x \leqslant 1$:

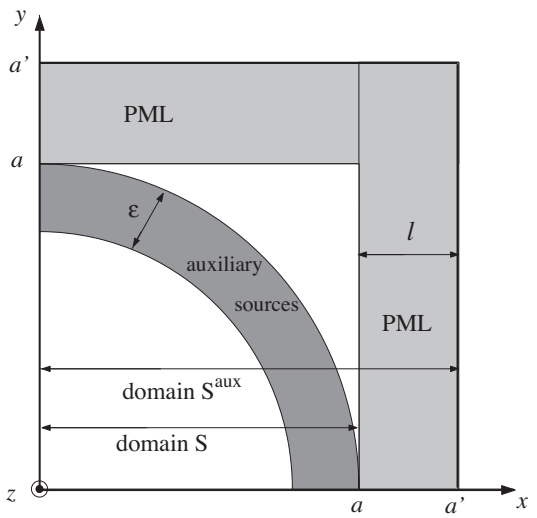

Fig. 3. Geometric setup. A two-dimensional section of the cube by the xy-plane.

$$P_4(x) = \begin{cases} 0, & x \leqslant 0, \\ 35x^4 - 84x^5 + 70x^6 - 20x^7, & 0 \leqslant x \leqslant 1, \\ 1, & x \geqslant 1. \end{cases}$$

The derivatives of $P_4(x)$ up to third order are equal to zero at the points $x = 0$ and $x = 1$. Therefore, the function $\mu(r)$ given by formula (45) increases smoothly from zero to one in the spherical layer $a - \varepsilon \leqslant r \leqslant a$ of width ε. The auxiliary currents are localized precisely in this layer, see Fig. 3. Indeed, when $r < a - \varepsilon$ we have $\mu(r) = 0$ and hence $\mathbf{j} = \mathbf{0}$ and $\mathbf{j}^{\mathrm{M}} = \mathbf{0}$, whereas for $r > a$ we have $\mu(r) = 1$ so that the interior problem transforms into the homogeneous Maxwell equations and the auxiliary currents vanish as well, see, e.g., formula (43).

Note that as we set up the computations using Cartesian coordinates, we could have also chosen the transition zone to be adjacent to the boundary ∂S from the inside. Then, there would have been no vacuum region between the transition zone and the PML, see Fig. 3. We will test this alternative configuration in the future.

Finally, as the solution to the AP clearly inherits the symmetry properties discussed in Section 6.1, relations (38)–(42) can be used in the capacity of the boundary conditions at the planes $x = 0$, $y = 0$, and $z = 0$. Namely, they help define the values of the solution at the ghost nodes according to the specific parity of every given field component at every given symmetry plane.

6.3. PML

The outer part $S^{\mathrm{aux}} \backslash S$ of computational domain S^{aux} is occupied by the PML of width $l = 0.75$ cm in each coordinate direction, see Fig. 3. For our computations, we take the unsplit PML derived by Zhao and Cangellaris in [58] for the Cartesian coordinate system. This PML is standard and well-known, and we present its governing equations in Appendix A. As the goal of this paper is to demonstrate the performance of the new stabilization technique based on quasi-lacunae, we use the original version of the PML [58] with no additional "fixes" reported in the literature.

6.4. Boundary conditions

At the outer boundaries $x = a'$, $y = a'$, and $z = a'$ of the domain S^{aux}, the PML itself is terminated either by zero Dirichlet boundary conditions for the tangential components of the magnetic field, or by a local artificial boundary condition. If the damping inside the layer is sufficiently strong, the boundary conditions at the outer boundaries of the PML do not affect the quality of the solution on S. The use of the ABC, however, may provide an additional benefit. In this case, if the layer is switched off (i.e., if $\sigma_x = \sigma_y = \sigma_z = 0$ everywhere), the boundaries still possess some non-reflecting properties sufficient for computing the solution with an acceptable accuracy. A computation of this kind (see Section 7) allows us to unambiguously attribute the undesirable long-time growth of the solution to the presence of the PML, because having the PML switched on or off appears the only difference between the two otherwise identical computational strategies.

The simplest local non-reflecting boundary condition at $\partial S^{\mathrm{aux}}$ can be taken in the form

$$\mathbf{H}^{\mathrm{aux}} = \mathbf{n} \times \mathbf{E}^{\mathrm{aux}}, , \tag{46}$$

where $\mathbf{n}$ is the unit normal vector to $\partial S^{\mathrm{aux}}$ in the outward direction. As the boundary $\partial S^{\mathrm{aux}}$ is composed of Cartesian planes, then in every given instance the vector $\mathbf{n}$ coincides with the corresponding unit vector $\mathbf{e}_x$, $\mathbf{e}_y$, or $\mathbf{e}_z$. Expression (46) involves the tangential components of the field vectors and holds for a plane wave propagating along $\mathbf{n}$. Without analyzing the non-reflecting properties of the ABC (46) to any degree of detail, we note that the flux of electromagnetic energy

$$\mathbf{S} = \frac{c}{4\pi}(\mathbf{E}^{\mathrm{aux}} \times \mathbf{H}^{\mathrm{aux}}) = \frac{c}{4\pi}|\mathbf{H}^{\mathrm{aux}}|^2\mathbf{n}$$

is directed outwards as long as (46) holds. In other words, the energy "drains out" of the computational domain thus aiding toward the stability of the algorithm.

As the ABC (46) is designed to absorb the plane waves that propagate normally to the boundary, it can be only an approximate radiation boundary condition. For the wave fronts that are not planar, or even for the plane waves but propagating in other directions, the ABC (46) will necessarily lead to partial reflections, see [1,2]. To somewhat reduce those reflections, we could have interpreted $\mathbf{n}$ in formula (46) as the unit radius vector, $\mathbf{n} = \mathbf{r}/|\mathbf{r}|$, rather than the unit normal to $\partial S^{\mathrm{aux}}$, because the wave fronts in the far field are nearly spherical. However, since the geometry we have chosen is Cartesian, and the design of local non-reflecting ABCs is not the primary focus of this paper, it is more convenient to use the simplest Cartesian version of (46), when $\mathbf{n}$ is the normal to $\partial S^{\mathrm{aux}}$, as long as the performance is acceptable for the current demonstration purposes (see Section 7).

6.5. Test solution

To study the performance of the algorithm, we need to be able to compute the actual numerical error on the grid at different moments of time. The explicit form of the reference solution that we use can be compactly written via field components in the spherical coordinate system (r, θ, φ):

$$E_r = \psi(r)\frac{2d_0\cos\theta}{r^3}\left(\chi + \frac{\dot\chi r}{c}\right) - \frac{d_0\cos\theta}{r^2}\left(\chi + \frac{\dot\chi r}{c} + \frac{\ddot\chi r^2}{c^2}\right)\frac{\partial\psi}{\partial r}, \tag{47}$$

$$E_\theta = \psi(r)\frac{d_0\sin\theta}{r^3}\left(\chi + \frac{\dot\chi r}{c} + \frac{\ddot\chi r^2}{c^2}\right), \tag{48}$$

$$H_\varphi = \psi(r)\frac{d_0\sin\theta}{cr^3}\left(\dot\chi r + \frac{\ddot\chi r^2}{c}\right). \tag{49}$$

This solution originates from the field radiated by a pointwise oscillating dipole $d(t) = d_0\chi(t)$ located at the origin of the coordinate system and oriented along the z-axis. The modulating function $\chi(t)$ is assumed smooth, and $\chi(t) \equiv 0$ for $t < 0$. To suppress the singularities in the origin, solution (47)–(49) is regularized by introducing a smooth multiplier $\psi(r)$ that should have at least three continuous derivatives at $r = 0$, leading to asymptotic behavior $\psi(r) = \mathcal{O}(r^3)$ as $r \to 0$. The components of the correspondent electric current that drives the solution (47)–(49) are:

$$j_r = \frac{d_0\cos\theta}{cr^2}\left(\dot\chi + \frac{\ddot\chi r}{c} + \frac{\dddot\chi r^2}{c^2}\right)\frac{\partial\psi}{\partial r}, \tag{50}$$

$$j_\theta = -\frac{d_0\sin\theta}{cr^3}\left(\dot\chi r + \frac{\ddot\chi r^2}{c}\right)\frac{\partial\psi}{\partial r}. \tag{51}$$

In Eqs. (47)–(51), the argument of the modulating function χ is the retarded time $\tau = t - r/c$, and the dot denotes differentiation with respect to time, e.g., $\dot\chi \equiv \frac{\partial\chi(t-r/c)}{\partial t}$. The solution given by formulae (47)–(49) obviously satisfies the symmetry constraints introduced in Section 6.1.

In Section 7, we solve system (32)–(37) with the right-hand sides (50) and (51) numerically (it is the interior problem, and the right-hand sides are transformed to the Cartesian coordinates), and evaluate the error by comparing the solution computed on the grid with the exact solution (47)–(49).

6.6. Discretization

Eqs. (32)–(37) that govern the solution to the interior problem are discretized on the grid with square cells: $h_x = h_y = h_z = h$ using the conventional second order accurate Yee scheme [9], see Appendix B. The AP of Section 6.2 is approximated using the same Cartesian grid and the same scheme. The AP grid extends to the entire domain S^{aux}, and involves the PML that terminates the interior domain S, see Fig. 3. Accordingly, the resulting discretization involves the discretization of the PML Eq. (64), see Appendix A, by means of the Yee scheme. The auxiliary ODEs (65) are approximated with second order accuracy on the same staggered grid. The PML itself is terminated either by the zero Dirichlet boundary condition or by the simple ABC (46), see Section 6.4. The thickness of the spherical layer $a - \varepsilon \leqslant r \leqslant a$, see Fig. 3, was about six grid cells in all our simulations. To demonstrate the grid convergence, we use a sequence of grids with $h = 0.15$, 0.075 and 0.0375 cm, see Section 7.

6.7. Time-marching

The discrete time-marching procedure is organized as follows. The Yee scheme updates the numerical solution in two stages. First, it advances the electric field in time. To do so, i.e., to update $(E_z)^n_{i+1/2,j+1/2,k}$ according to Eq. (66), the magnetic field needs to be known on the entire grid including the boundary values of the tangential components $(H_y)^{n+1/2}_{N,j+1/2,k}$ and $(H_x)^{n+1/2}_{i+1/2,N,k}$ at the planes $x = a$ and $y = a$, i.e., at $i = N$ and $j = N$, respectively. Next, the magnetic field is updated, see Eq. (67). However, this update can be done only inside the computational domain and not at the boundary. Indeed, the boundary values $(H_x)^{n+1/2}_{i+1/2,N,k}$ cannot be updated according to (67) as it would require the knowledge of the electric field E_z outside the computational domain. Likewise, the boundary values $(H_y)^{n+1/2}_{N,j+1/2,k}$ cannot be updated using the discrete counterpart of Eq. (36). As the tangential components of the magnetic field at the boundary become unavailable at the next time level, the next full update of the electric field will not be possible either. Therefore, an alternative procedure is needed for defining the tangential components of the magnetic field at the boundary planes $x = a$, $y = a$, and $z = a$ at each time level. The alternative procedure that we propose exploits the split into the interior and auxiliary sub-problems (Section 5) and the integration of the AP using quasi-lacunae (Sections 2 and 4).

Assume that we have updated the electric and magnetic field as outlined above, and obtained the values of $\mathbf{E}^{n+1}$ and $\mathbf{H}^{n+3/2}$ everywhere on the interior grid except at the boundary, where the magnetic field has not been updated. Then, we can multiply the resulting $\mathbf{E}^{n+1}$ and $\mathbf{H}^{n+3/2}$ by the function μ of (45) and define the auxiliary currents as follows:

$$\frac{4\pi}{c}(j_z)^{n+1/2}_{i+1/2,j+1/2,k} = -\frac{1}{c}\frac{(\mu E_z)^{n+1}_{i+1/2,j+1/2,k} - (\mu E_z)^{n}_{i+1/2,j+1/2,k}}{\tau} + \frac{(\mu H_y)^{n+1/2}_{i+1,j+1/2,k} - (\mu H_y)^{n+1/2}_{i,j+1/2,k}}{h_x} - \frac{(\mu H_x)^{n+1/2}_{i+1/2,j+1,k} - (\mu H_x)^{n+1/2}_{i+1/2,j,k}}{h_y}, \tag{52}$$

$$\frac{4\pi}{c}\left(j_x^{\mathrm{M}}\right)^{n+1}_{i+1/2,j+1/2,k} = \frac{1}{c}\frac{(\mu H_x)^{n+3/2}_{i+1/2,j,k} - (\mu H_x)^{n+1/2}_{i+1/2,j,k}}{\tau} + \frac{(\mu E_z)^{n+1}_{i+1/2,j+1/2,k} - (\mu E_z)^{n+1}_{i+1/2,j-1/2,k}}{h_y} - \frac{(\mu E_y)^{n+1}_{i+1/2,j,k+1/2} - (\mu E_y)^{n+1}_{i+1/2,j,k-1/2}}{h_z}. \tag{53}$$

Note that the unknown boundary values of the (tangential) magnetic field are not required to compute the auxiliary currents since the latter differ from zero only in the transition zone, see Fig. 3, and vanish, in particular, at the outer boundary of S.

Having obtained the auxiliary currents $\mathbf{j}$ and $\mathbf{j}^{\mathrm{M}}$ that drive the AP, see formulae (52) and (53), we can advance the discrete solution to the AP by one time step. This can be done everywhere on S, including the boundaries, because the AP is terminated by the PML outside S. And as the solutions to the interior and auxiliary problems coincide at the boundaries $x = a$, $y = a$, and $z = a$, we can recover the tangential components of the magnetic field needed for the interior problem. Therefore, the solution to the interior problem can be advanced further in time by one additional step, and the procedure cyclically repeats itself.

The key consideration is that the AP is time-marched with the help of quasi-lacunae, as described in Sections 2 and 4. In other words, what we actually integrate in time is those partial problems of type (1) and (2), (12), terminated by the PML, that have not yet reached their respective steady states on S, and hence still need to be carried on. For every given moment of time t, these are the partial problems $i = N_0, \ldots, N_1$, see formula (14), where N_0 and N_1 individually depend on t, but their difference $N_1 - N_0$ remains bounded by a fixed quantity for all times.

In practice, one may either solve the partial problems (1), (2), (12) individually, or time-march the solution of the AP in its entirety. In any event, once the lower limit of summation $N_0 = N_0(t)$ in formula (14) becomes larger than the index i of a given partial problem, the solution of the latter, $\mathbf{E}_i$ (and $\mathbf{H}_i$), must be excluded from the overall sum and must remain excluded continuously thereafter. If the solution of the AP is marched in its entirety, this can be done by recomputing and then subtracting the contribution for a given i from the overall solution of the AP.

In addition to the unsteady components $\mathbf{E}_i$ (and $\mathbf{H}_i$), the overall solution of the AP on S contains the steady-state part, $\mathbf{E}^{\mathrm{st}}$ (and $\mathbf{H}^{\mathrm{st}}$), see (14). One can obtain $\mathbf{E}^{\mathrm{st}}$ and $\mathbf{H}^{\mathrm{st}}$ by solving the Poisson equations (9) and (10), subject to the appropriate ABC at ∂S. Alternatively, one can obtain $\mathbf{E}^{\mathrm{st}}$ and $\mathbf{H}^{\mathrm{st}}$ with the help of the same time-depended scheme (Yee scheme) as used for integrating the Maxwell equations, merely as the solution that forms inside the quasi-lacuna once the unsteady waves have left the computational domain. We adopt the second approach in the current paper as it has proven efficient in practice, see the discussion around Eq. (61).

Let us note that having the correct steady-state components $\mathbf{E}^{\mathrm{st}}$ and $\mathbf{H}^{\mathrm{st}}$ in the overall solution of the AP is important only when this solution is used to provide the boundary data for the interior problem. For time-marching the AP per se, what matters is only to let the unsteady components of the solution out of the computational domain. The steady-state component does not evolve between the updates by its very nature, and does not need to be time-marched. Therefore, when the contribution for a given i is removed, it can be removed from the solution of the AP completely, i.e., both the unsteady part, as well as the steady-state one. The steady-state component is subsequently brought back, but only when setting the boundary conditions for the interior problem.

In Fig. 13 (see p. 36), we are showing the block diagram of the entire algorithm. In Section 6.8, we discuss some additional implementation details for the discrete formulation.

6.8. Additional implementation details

Partitioning of the RHS to the AP according to formula (12) may appear problematic in the discrete setting, because each partial source $\mathbf{j}_i$, $\mathbf{j}_i^{\mathrm{M}}$ is turned on and off abruptly. The resulting discontinuities at $t_i = iT_0$ will lead to the loss of consistency by the scheme and to "smearing out" of the sharp aft fronts of the outgoing waves. Therefore, following our previous analysis [21–23], we introduce a "smooth" approach to the partitioning of the RHSs $\mathbf{j}$ and $\mathbf{j}^{\mathrm{M}}$.

Let us consider a smooth partition of unity on the semi-infinite interval $t \geqslant 0$:

$$\forall t \geqslant 0: \quad 1 = \sum_{i=0}^{\infty} \zeta(t - (i-1)T_1), \quad \operatorname{supp}\zeta(t) = [T_1 - \Delta T, 2T_1], \tag{54}$$

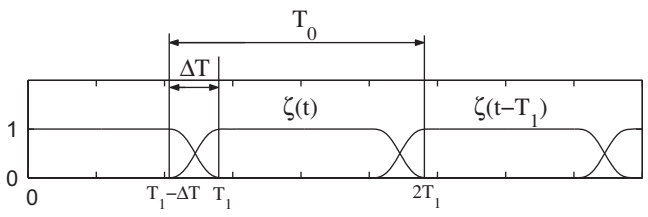

Fig. 4. A smooth partition of unity.

as schematically shown in Fig. 4. Here T_0 is the size (duration) of each partition element (as in Section 2), ΔT is the width (duration) of the overlapping interval, and

$$T_1 \stackrel{\text{def}}{=} T_0 - \Delta T. \tag{55}$$

We denote by $\zeta(t)$ a smooth compactly supported function that defines the partition so that $\zeta(t) \equiv 1$ for $T_1 \leqslant t \leqslant 2T_1 - \Delta T$ and $\zeta(t) + \zeta(t + T_1) \equiv 1$ for $T_1 - \Delta T < t < T_1$. The individual partition elements are obtained by a mere translation: $\zeta(t - (i-1)T_1)$, $i = 0, 1, 2, \ldots$

Multiplying the continuously operating currents $\mathbf{j}$ and $\mathbf{j}^{\mathrm{M}}$ by the sum given in formula (54), we obtain [cf. formula (12)]:

$$\begin{aligned} \mathbf{j}(\mathbf{x},t) &= \sum_{i=0}^{\infty} \mathbf{j}_i(\mathbf{x},t), \quad \mathbf{j}_i(\mathbf{x},t) = \mathbf{j}(\mathbf{x},t)\zeta(t-(i-1)T_1), \\ \mathbf{j}^{\mathrm{M}}(\mathbf{x},t) &= \sum_{i=0}^{\infty} \mathbf{j}_i^{\mathrm{M}}(\mathbf{x},t), \quad \mathbf{j}_i^{\mathrm{M}}(\mathbf{x},t) = \mathbf{j}^{\mathrm{M}}(\mathbf{x},t)\zeta(t-(i-1)T_1), \end{aligned} \tag{56}$$

so that for each $i = 0, 1, 2, \ldots$ the partitioned RHSs (56) are compactly supported on the domain

$$Q_i = \{(\mathbf{x},t) | \mathbf{x} \in S, iT_1 - \Delta T < t < (i+1)T_1\}. \tag{57}$$

Unlike in the case of partition (12), the functions (56) are smooth in both space and time. Hence, the finite-difference scheme is now expected to reproduce the quasi-lacunae phenomenon for each partial problem with its design accuracy. Moreover, because of the overlap ΔT that partition (56) has and partition (12) does not, both the moment $t_0^{(i)}$ of inception of the ith partial source, as well as the moment $t_2^{(i)}$, when the domain S falls completely into the quasi-lacuna of the solution due to this source, need to be redefined compared to formulae (13). Namely, instead of (13a) we now have:

$$t_0^{(i)} \stackrel{\text{def}}{=} iT_1 - \Delta T, \tag{58a}$$

where T_1 is defined by (55) (except for $i = 0$, for which $t_0^{(i)} = 0$), and (13b) is replaced by

$$t_2^{(i)} \stackrel{\text{def}}{=} t_0^{(i)} + T_{\text{int}}, \tag{58b}$$

where $t_0^{(i)}$ has a new definition (58a), and T_{int} is still given by (11a).

Given the partition (56), the ith partial subproblem is included into the calculation at $t_0^{(i)}$ defined by (58a) and is dropped at $t_2^{(i)}$ defined by (58b), when the solution reaches the steady state on the domain of interest S. Similarly to Section 2, the interval between the termination time $t_1^{(i)} \stackrel{\text{def}}{=} (i+1)T_1$ of the ith partial current, see formula (57), and the moment of time $t_2^{(i)}$ is equal to $\frac{1}{c}\operatorname{diam} S$"seconds," which is the time needed for the waves to leave the domain S.

When the lacunae-based algorithm of Section 2 is applied to a Huygens' problem, it needs the accumulated charges $\rho(\mathbf{x},t)$ and $\rho^{\mathrm{M}}(\mathbf{x},t)$ as the source terms of Eqs. (9) and (10), respectively. These accumulated charges enable the computation of the steady-state contribution to the overall solution. For the partition of unity (54), the electric charge accumulated during the time period $0 < t < t_1^{(N_0-1)}$ due to operation of the first N_0 partial currents $\mathbf{j}_i$, $i = 0, \ldots, N_0 - 1$, is expressed as

$$\rho(\mathbf{x}, t_1^{(N_0-1)}) = \rho(\mathbf{x}, N_0T_1 - \Delta T) - \int_{N_0T_1-\Delta T}^{N_0T_1} \operatorname{div} \mathbf{j}(\mathbf{x},t)\zeta(t-(N_0-2)T_1)dt, \tag{59}$$

and similarly for the magnetic charge and the corresponding magnetic currents $\mathbf{j}_i^{\mathrm{M}}$. The first term on the right-hand side of (59) represents the charge accumulated during the period $0 < t < N_0T_1 - \Delta T$, whereas the integral adds the charge accumulated during the "decline" phase (see Fig. 4) of the last partial current, $\mathbf{j}_{N_0-1}$. As long as $\rho(\mathbf{x},t)$ can be considered a given function of space and time, it is only the integral term in (59) that needs to be evaluated numerically. Numerical integration may, in principle, introduce some additional error on the right-hand side of Eqs. (9) and (10), but as the length of the integration interval in formula (59) is fixed and equal to ΔT, estimate (26) will still hold, except that the constant C_2 formally becomes a function of ΔT:

$$\left\| \tilde{\mathbf{w}}_{N_0}^{(S),\mathrm{st}}(\mathbf{x}) - \mathbf{w}_{N_0}^{(S),\ \mathrm{st}}(\mathbf{x}) \right\| \leqslant C_2(\Delta T)\|\boldsymbol{\psi}\|''. \tag{60}$$

As such, the overall error estimate (27) will hold as well, again, with $C_2(\Delta T)$ substituted for C_2.

For the non-Huygens' formulation of Section 5 though, only the currents $\mathbf{j}(\mathbf{x},t)$ and $\mathbf{j}^{\mathrm{M}}(\mathbf{x},t)$ can be considered given functions of space and time,[5] whereas the charges $\rho(\mathbf{x},t)$ and $\rho^{\mathrm{M}}(\mathbf{x},t)$ are not defined independently. Consequently, the first term on the right-hand side of formula (59) needs to be evaluated numerically as well. This approach may be prone to the accumulation of error as it involves the integration of the continuity equation (5) between $t = 0$ and $t = N_0T_1 - \Delta T$.

In the actual computations however, we do not solve the Poisson equations (9) and (10) explicitly. We rather employ an alternative approach and use the steady-state solution computed by the same Yee scheme. It develops and stays on S after all the unsteady waves leave. Let $\mathbf{E}_i = \mathbf{E}_i(\mathbf{x},t)$ denote the electric field due to the partition element i, as in Section 2. Then, at

[5] The currents are computed based on the interior solution in the course of the combined time-marching, see formulae (52) and (53), yet from the standpoint of solving the AP they are interpreted as given functions.

$t \geqslant t_2^{(i)}$ it reaches the steady state on the domain S and remains unchanged continuously thereafter, i.e., $\mathbf{E}_i(\mathbf{x}, t) = \mathbf{E}_i^{\mathrm{st}}(\mathbf{x})$ for all $t \geqslant t_2^{(i)}$ and $\mathbf{x} \in S$. Hence, the overall steady-state contribution to the solution of the AP at the moment of time t is given by

$$\mathbf{E}^{\mathrm{st}}(\mathbf{x}) = \sum_{i=0}^{N_0-1} \mathbf{E}_i^{\mathrm{st}}(\mathbf{x}), \quad \mathbf{x} \in S, \tag{61}$$

where $N_0 = N_0(t)$ is defined in Section 2. This approach to evaluating $\mathbf{E}^{\mathrm{st}}(\mathbf{x})$ does not involve the integration of the continuity equation. It may still be prone to the accumulation of error though because in formula (61) the steady-state contributions from all the elements of the partition (56), starting with $i = 0$, are summed up. Yet the error growth may not be faster than linear with respect to N_0, because all individual errors associated with individual terms of the sum (61) are bounded, see formula (24). In practice, the behavior of the method was even more favorable, as no accumulation of error associated with the use of formula (61) has been observed at all, see Section 7. This suggests that a theoretical analysis of this case (the currents are given but the charges are not) may in the future lead to a uniform estimate similar to that given by Theorem 1.

In addition, let us re-emphasize that even though the partition of the source terms in time (electric and magnetic currents) presented in Fig. 4 is the same as we used in our prior work, see, e.g., [25], the current approach is fundamentally different from the previous one. In [25], we have indicated that lacunae-based integration can help stabilize an ABC or a PML for a non-Huygens' problem, but have never implemented the idea because it required the solenoidal (i.e., divergence-free) auxiliary currents. Those auxiliary currents were built and tested earlier for standalone lacunae-based ABCs, see Section 3 and [24] for detail, but it was a rather cumbersome and non-trivial component of the algorithm. In the current paper, we are using quasi-lacunae instead of the conventional lacunae, and hence the auxiliary currents do not have to be solenoidal, see formula (43). This presents a major simplification over both [24,25].

7. Results of computations

For our numerical experiments, we take $\psi(r) = 1 - \exp(-r^5)$ in formulae (47)–(49). This guarantees that the fields are smooth and bounded at the origin: $E_r \sim r^2$, $E_\theta \sim r^2$, and $H_\varphi \sim r^3$. Moreover, due to the exponential decay of the derivative $\psi'(r) = 5r^4\exp(-r^5)$ the external currents (50) and (51) appear essentially confined to the domain S. We also take $d_0 = 1$ in Eqs. (47)–(51).

The modulating function $\chi(t)$ is chosen as

$$\chi(t) = \begin{cases} \sin^4 \omega_1 t + \sin^4 \omega_2 t, & \text{if } t \geqslant 0, \\ 0, & \text{if } t < 0, \end{cases} \tag{62}$$

where the frequencies ω_1, ω_2 are incommensurate, $\omega_1 = 1/2, \omega_2 = \omega_1/\sqrt{2}$, so that the solution is not periodic in time. The function $\chi(t)$ of (62) and its derivatives up to order 3 are continuous at $t = 0$:

$$\chi(0) = \dot{\chi}(0) = \ddot{\chi}(0) = \dddot{\chi}(0) = 0.$$

We will first demonstrate the onset of instability in the original PML — the particular effect that we would like to have suppressed by our methodology. For that purpose, we numerically solve the Maxwell equations (32)–(37) on the domain S, and terminate this domain by the PML (64), (65) so that the entire computation is run on the domain S^{aux}, see formula (44) and Fig. 3. The solution is driven by the external currents (50) and (51) and hence the exact solution (47)–(49) is available for comparison. We emphasize that this is a reference computation for which we need neither the decomposition into the interior and auxiliary sub-problems nor the temporal partition. The width of the PML is fixed to 0.75 cm on every grid we use, which means that the number of cells in the layer increases as the grid size h decreases. The magnitude of the damping coefficient is $\sigma_0 = 10$, see Section 6.3. The PML is terminated by the simple ABC (46).

In Fig. 5, we are showing the binary logarithms of the error in E_x as functions of time for three grids with square cells: $h = 0.15$, 0.075, and 0.0375 cm. The error in Fig. 5, as well as in Figs. 6–10, is defined as *the relative error*, i.e., as the difference between the numerical solution and the exact solution (47)–(49) divided by the magnitude of the exact solution. It is evaluated on the domain S in the maximum norm (L_∞). The computations are run until $ct = 105$, which corresponds to about 12 times the time required for the waves to cross the domain S.

At the beginning stage of the computation, the numerical solution exhibits the design rate of grid convergence, $\mathcal{O}(h^2)$, see the enlarged plot in Fig. 5(b). However, at a certain moment of time the error starts to increase very rapidly. The rate of this increase is nearly the same for all grids, but on the finest grid the blow-up is somewhat delayed, see Fig. 5(a). When the norm of the error reaches a certain level (e.g., the logarithm is equal to roughly 15 on the grid with $h = 0.075$), we call is a complete loss of accuracy and stop the computation.

We also note that the initial spike of the error appears in Fig. 5 because what is actually plotted is the relative error, and the exact solution (47)–(49) is very small at the beginning stage of the computation due to our choice of the modulating function $\chi(t)$, see formula (62).

In Fig. 6, we are showing the error profiles with the PML switched off, i.e., with $\sigma_x = 0$, $\sigma_y = 0$, and $\sigma_z = 0$ everywhere in the layer, so that the computational domain is terminated only by the ABC (46). Otherwise, the setup is identical to that of Fig. 5. We see that the error curves in Fig. 6 differ from those in Fig. 5 in two key aspects. On one hand, the $\mathcal{O}(h^2)$ grid convergence

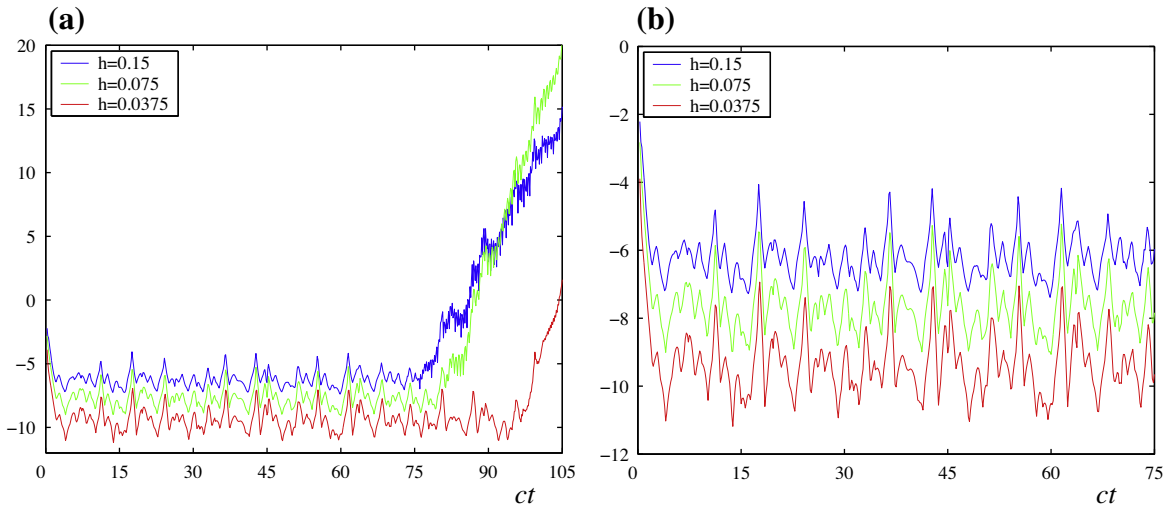

Fig. 5. Computation with the PML (64). Binary logarithm of the maximum norm error for E_x vs. time.

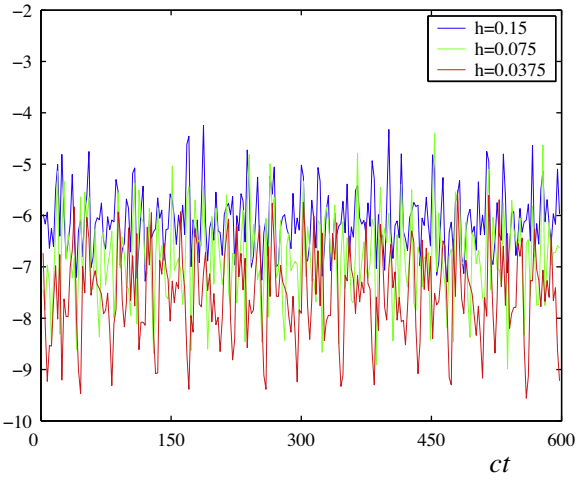

Fig. 6. Computation with the ABC (46). Binary logarithm of the maximum norm error for E_x vs. time.

can hardly be identified in Fig. 6; in particular, there is basically no difference in the absolute value of the error between $h = 0.075$ and $h = 0.0375$. The reason for that is obvious. The error inside the computational domain S is dominated by reflections from the outer boundaries $x = a'$, $y = a'$, and $z = a'$, and the magnitude of those reflections is not related to the grid size. In other words, the accuracy of the local first order ABC (46) appears worse than that of the interior scheme. On the other hand, in sharp contrast to Fig. 5, the errors in Fig. 6 stay bounded for all times, and there is no growth. As the PML is the only difference between the two setups, we conclude that the deterioration of the numerical solution observed in Fig. 5 should unambiguously be attributed to the presence of the PML. Note that the computation interval $ct = 600$ corresponds to about 70 times the time required for the waves to cross the domain S.

To avoid any potential inaccuracies, in Fig. 7 we present the same error profiles as in Figs. 5 and 6, except that the PML and no-PML error curves for every grid are given on a separate plot. We conclude that on the coarsest grid, $h = 0.15$, see Fig. 7(a), the overall error is dominated by that of the interior discretization, because the two curves are nearly identical at the beginning of the calculation, but at a later stage the PML solution deteriorates. On finer grids, see Fig. 7(b) and (c), the accuracy of the PML solution at the initial stage improves as the grid size decreases, which is an indication of grid convergence, but later the instability of the PML kicks in. At the same time, the error curves for artificial boundary conditions (46) remain "flat" for all times, but the accuracy does not improve as the grid is refined due to the reflections from the outer boundaries.

Prior to presenting the results of computations with quasi-lacunae, we note the following:

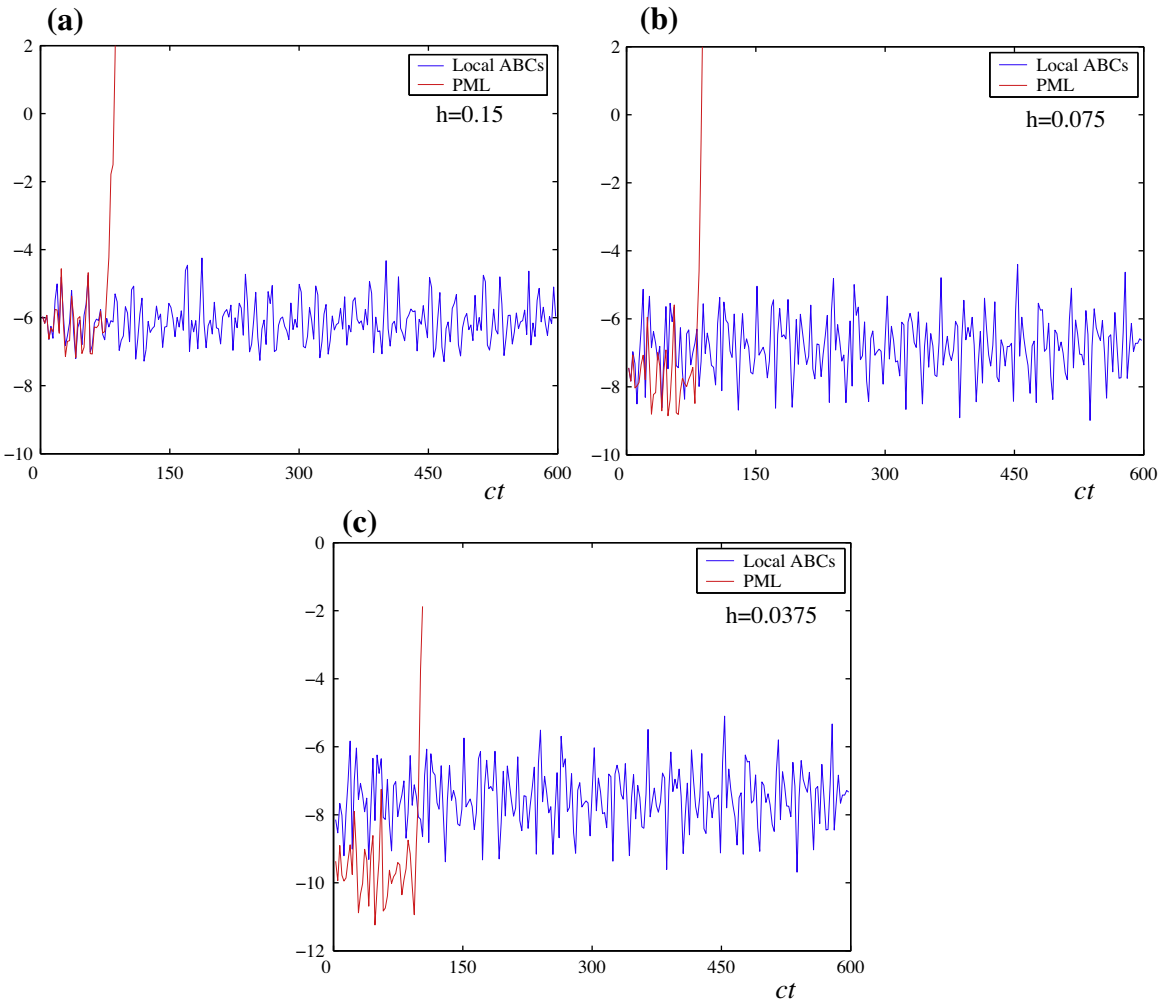

Fig. 7. PML (64) and (65) vs. ABC (46) on different grids. Binary logarithm of the L_∞-norm error for E_x vs. time.

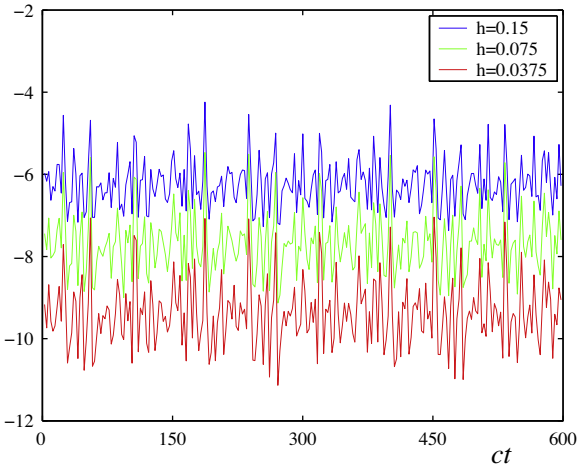

Fig. 8. Computation with the PML and quasi-lacunae. Binary logarithm of the L_∞-norm error for E_x vs. time.

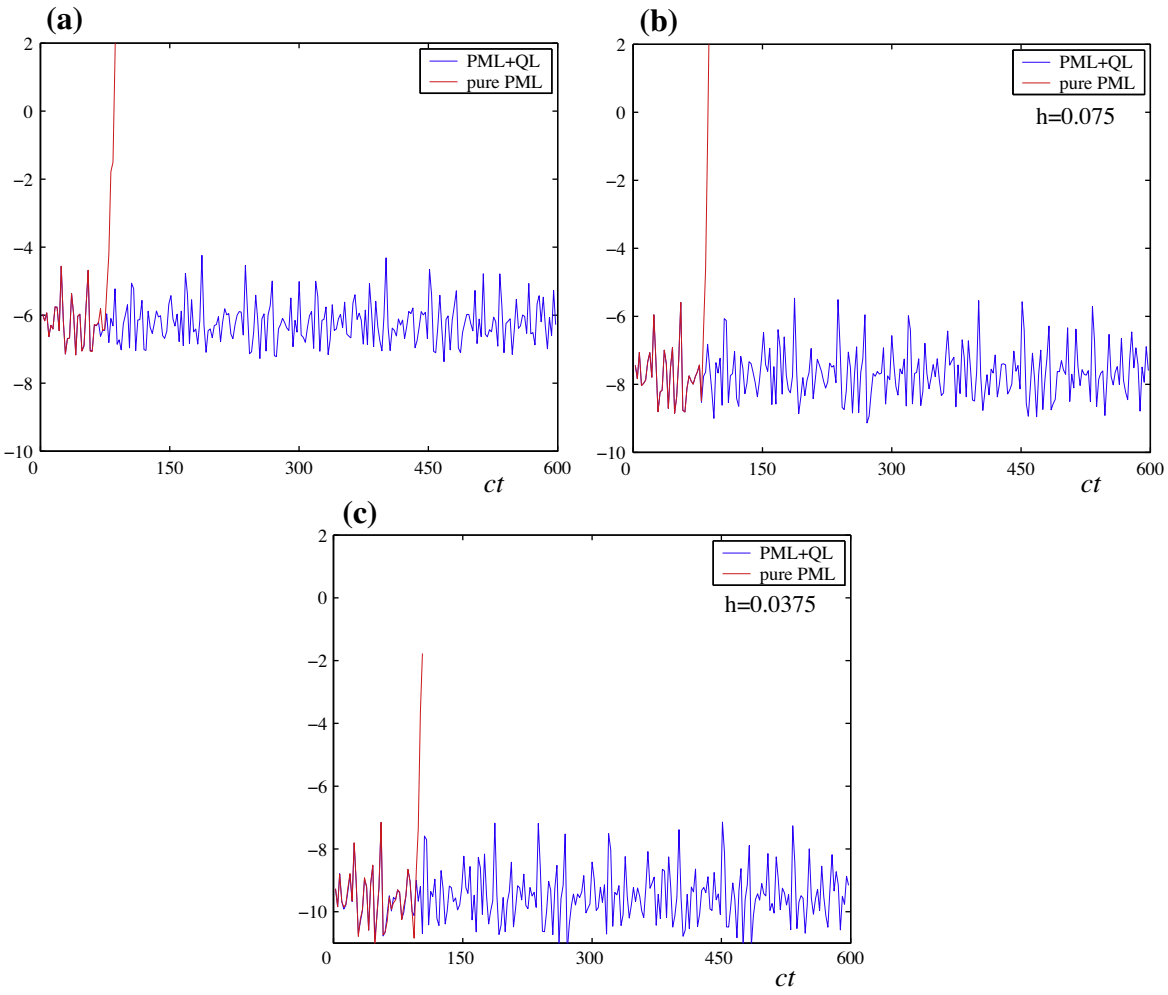

Fig. 9. PML and quasi-lacunae vs. PML on different grids. Binary logarithm of the L_∞-norm error for E_x vs. time.

- The error profiles for E_y, E_z, H_x, and H_y are very similar to those for E_x (including the case with quasi-lacunae case reported below), and hence we do not present them hereafter.
- We have observed in our experiments that the decrease of the damping coefficient σ inside the PML could somewhat extend the interval of time before the onset of the error build-up, and vice versa, the increase of σ helps shorten this interval of time. However, reducing σ cannot be considered a good remedy for mitigating the instability generated by the PML because on one hand the error build-up occurs anyway, albeit a bit later, and on the other hand, if σ is too small, then the PML does not guarantee a sufficient damping of the outgoing waves, and the overall accuracy is affected by the boundary conditions set at its outer boundaries.
- We have also conducted computations with the zero Dirichlet boundary conditions that replace the ABC (46) at the outer boundary of the PML. The results were practically indistinguishable from those shown in Fig. 5. Hence, we conclude that as long as the damping in the layer is sufficient, the outer boundary condition has little effect on the solution.
- Prior to computing the solution in the Cartesian coordinates, we have also computed it in the spherical coordinates, with only three rather than five field components in the TM mode, see Sections 6.1 and 6.5. We have used the unsplit spherical PML of [59] that was derived from the same principles as the Cartesian PML (64) and (65). However, we did not see any signs of instability or accuracy loss in the spherical case. The likely reason is that the spherical PML is uni-directional, whereas the Cartesian PML has edge and corner regions that are apparently more susceptible to the development of instabilities.
- The initial spike of the error, which can be seen in Fig. 5 and which we attribute to the fact that this is relative error, cannot be observed in either Figs. 6 or 7 merely because of a lower plotting resolution. Namely, to graphically represent the data for the abscissa range of $[0,600]$ (Figs. 6 and 7), as opposed to $[0,105]$ (Fig. 5(a)), we coarsen the original dataset by keeping only every eighth point for $h = 0.15$, every sixteenth point for $h = 0.075$, and every thirty second point for $h = 0.0375$, and leaving out all others.

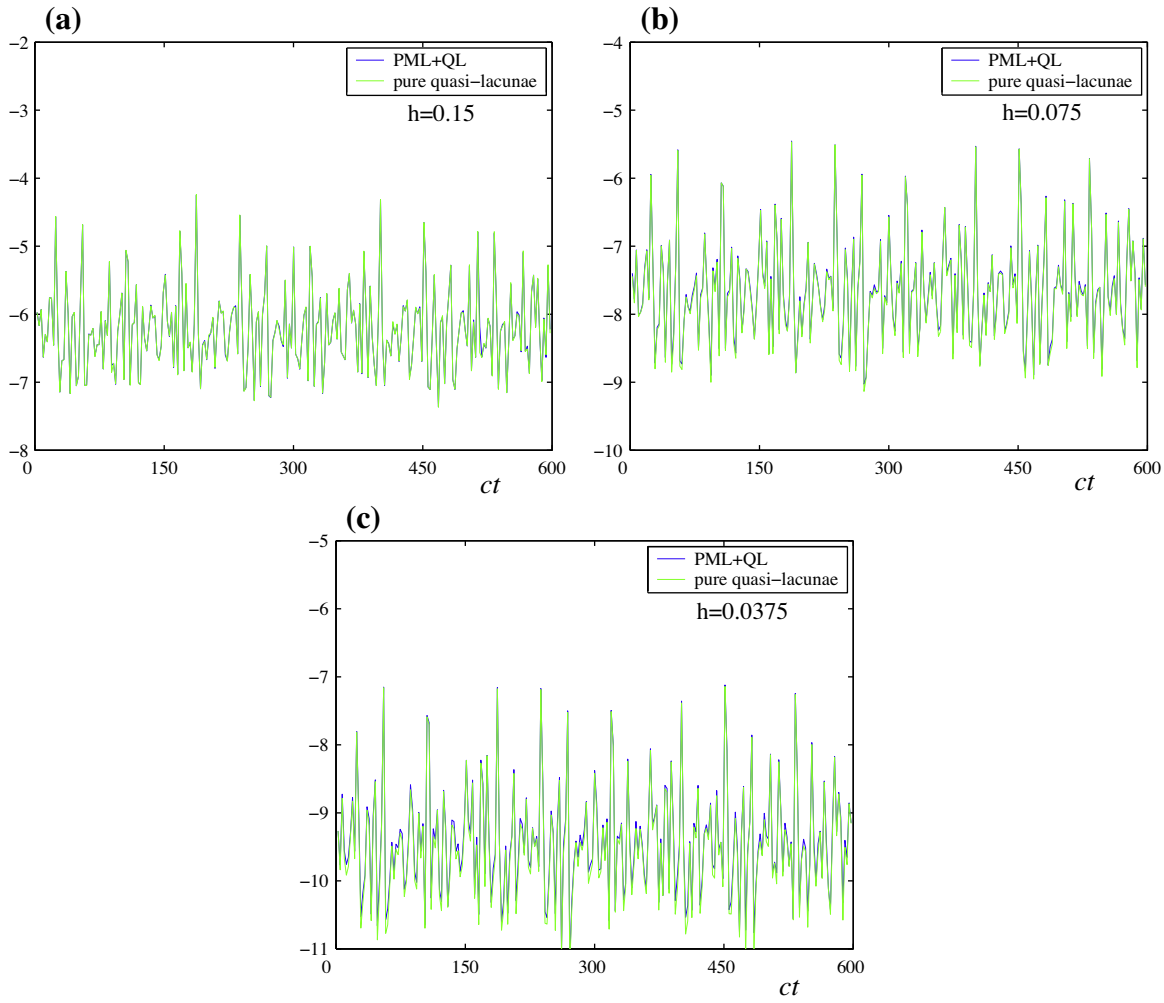

Fig. 10. Quasi-lacunae vs. PML and quasi-lacunae on different grids. Binary logarithm of the L_∞-norm error for E_x vs. time.

Let us now proceed to presenting the main experimental result of the paper. Namely, we will show that having the PML enhanced by the time-marching based on quasi-lacunae completely eliminates the long-time deterioration of the numerical solution.

We choose the following parameters of the temporal partition: $cT_0 = 10$ diam$S \approx 42$ cm (where $c = 1$ is the speed of light, and diam$S = \sqrt{3}a \approx 4.2$ cm, see Fig. 3) and $c\Delta T = 0.1cT_0 = 4.2$ cm. For these parameters, the number of partial problems (1), (2), (12) that may overlap at any given moment of time never exceeds two. The actual percentage of time with the overlap (as opposed to the time when only one partial problem needs to be integrated) is

$$\frac{\frac{1}{c}\text{diam } S + \Delta T}{T_0 - \Delta T} \approx 22\%. \tag{63}$$

We will see that this quantity is related to the overhead of the proposed computational procedure.

In Fig. 8, we are showing the results of computations for exactly the same setup as the one that corresponds to Fig. 5, except that the solution is time-marched with the help of quasi-lacunae. We see that the long-time deterioration is eliminated, and as the grid size decreases, the numerical solution converges to the exact one with the design rate, $\mathcal{O}(h^2)$, for the entire duration of integration. In Fig. 9 we are showing the same error profiles as in Figs. 8 and 5(a), except that the "only PML" curve and the "PML and quasi-lacunae" curve for each individual grid are presented on a separate plot. This allows us to use the same scale. We see that at the initial stage of computation the two error curves coincide on each grid, and also that the actual values of the error decrease with second order accuracy as the grid is refined. Later, the pure PML solutions blow up whereas the solutions computed with the help of quasi-lacunae maintain their stability for as long as the computation is run.

Finally, we compare the results obtained using the combination of quasi-lacunae and the PML with those obtained using quasi-lacunae as the sole termination of the computational domain. This approach, as described in Section 3, requires a wider buffer zone around the computational domain S compared to the PML, and consequently, the computations are more expensive. Yet this method introduces no error associated with the domain truncation, and the only source of error on S is the interior discretization. In Fig. 10, we compare the error profiles for the pure quasi-lacunae case with those for the quasi-lacunae and PML case on different grids.

We see that the two curves nearly coincide for each grid. Hence, the error on S obtained using the combined quasi-lacunae and PML methodology is the same as that for the pure quasi-lacunae based approach. As the latter is due to the interior discretization only, we conclude that the accuracy of the boundary procedure offered by the combined quasi-lacunae and PML methodology already exceeds the accuracy of the scheme on S and consequently, the overall accuracy cannot be further improved by changing the treatment of the outer boundary.

Let us now assume that the complexity of solving the original problem with the PML and with no lacunae-based correction (the "baseline" computation presented in Fig. 5) is $A + P$ units of cost *per unit time,* where A is the cost of integrating inside the domain S, P is the cost of applying the PML on $S^{\text{aux}} \setminus S$, see Fig. 3, and the unit of cost may be a flop or a CPU second or any other appropriate measure. The original procedure, however, cannot be used for integrating over arbitrarily long time intervals, because it blows up. Therefore, it is supplemented by the lacunae-based correction. Let us assume for simplicity that the cost of integrating the AP on S is also A per unit time, then the overall complexity for one interior problem and one AP solved simultaneously will be $2A + P$, because the PML is used only for the AP. This is the theoretical minimum cost, which can be used as a reference. However, solving the interior problem along with only one AP at every given moment of time is not sufficient for correcting the long-time deterioration, because it does not allow to apply the lacunae-based integration to the AP. To allow for that, there must be an overlap between the APs, and for our current implementation this overlap was 22%, see formula (63). In other words, we were solving two APs simultaneously for 22% of the time and one AP for the rest of the time. Consequently, the total cost was $A + 1.22(A + P)$ per unit time. The overhead can then be defined as the ratio of the actual cost to the reference minimum cost, which corresponds to the limit of the zero overlap:

$$\frac{A + 1.22(A + P)}{2A + P}.$$

Alternatively, one can think of the overhead as the ratio of the actual cost to the cost of solving the original problem with the PML:

$$\frac{A + 1.22(A + P)}{A + P}.$$

The second measure is somewhat less representative in our view because the reference cost of $A + P$ pertains to the algorithm that does not work over long times at all, whereas the reference cost $2A + P$ corresponds to the theoretically minimal amount of correction.

Let us also note that a more traditional way of looking at complexity is to measure everything in terms of the grid dimension, see [2, Section 3.7], and relate the cost to the error. Along these lines, we can say that for the implementation tested in the current paper both A and P are proportional to h^{-4}, where h is the size of the spatial discretization. This, however, is not sufficient for understanding the complexity of the proposed procedure. Indeed, traditionally we estimate the cost of a method on a given fixed interval of time assuming that it produces the solution of a reasonable quality. In doing so, we are interested to see how the cost of implementation depends on various parameters of the method and on the required final accuracy. Here, on the other hand, the baseline method is assumed to perform well only over some limited interval of time, after which it blows up. Hence, the goal is to have its original accuracy restored for arbitrarily long times. Therefore, we do not need to relate the complexity to accuracy, because this relation is already built into the definition of the baseline method over the time of its acceptable performance. We rather need to compare the actual cost of having the baseline method corrected for long times with the theoretically minimum possible cost. Of course, in this context we are talking about a universal correction, as opposed to various specific corrections that apply to specific methods, see Section 1.

8. Discussion

We have built and tested a special time-marching algorithm for the numerical integration of unsteady electromagnetic problems. It exploits the presence of quasi-lacunae in the solutions of Maxwell's equations, and can be applied to any discretization of these equations on the grid. For Huygens' problems driven by known sources (electric and/or magnetic currents and charges), our algorithm guarantees that the error on a given grid will stay bounded for all times. When the grid size decreases, the error will also decrease with the design rate of the scheme. Moreover, it will decrease uniformly in time, which is equivalent to having a temporally uniform grid convergence.

A more realistic problem formulation would typically involve the radiation of waves toward infinity, but altogether will not necessarily be Huygens'. In that case our methodology can be combined with an appropriate procedure used for the treatment of the artificial outer boundary, such as an ABC or a PML. Through the decomposition of the original problem into the interior and auxiliary sub-problems, it provides for a uniform non-deteriorating performance of the chosen ABC or PML for all times, without compromising any of its original properties, such as the accuracy or degree of absorption. In other

words, our methodology prevents the loss of accuracy/stability by the ABC or PML over long integration times — an adverse phenomenon reported by different authors in the literature. In doing so, only the far-field part of the overall formulation must satisfy the (generalized) Huygens' principle, whereas inside the computational domain, i.e., in the near field, the model may not be Huygens' at all.

We emphasize that the proposed algorithm will correct the long-time behavior of any ABC or PML. An important question in this context is at what level will the error eventually stabilize. Our central theorem, Theorem 1 of Section 4, only requires that the growth of the error that characterizes the original non-modified ABC or PML be controlled by some function $\eta = \eta(t)$, but imposes essentially no constraints on η. For example, in Section 7 we saw that $\eta(t)$ may show no evidence of growth at an early stage of the computation, but may then display a sharp explosive error buildup. After the new time-marching algorithm is applied, the error stabilizes at the level $\sim\eta(T_{\text{int}})$, where T_{int} is bounded from below by the time needed for the waves to cross the computational domain. T_{int} may also be chosen greater than $\frac{1}{c}\operatorname{diam} S$ (see Section 7), which potentially increases the error but reduces the computational overhead that the new procedure entails. Hence, we can always think about striking the right balance between the overhead and the final accuracy. As to whether or not the error $\sim\eta(T_{\text{int}})$ for the chosen T_{int} is acceptable in a given setting, it obviously depends on the specific application. Consequently, the choice of T_{int} or equivalently, the choice of the partition shown in Fig. 4, shall be made based on the experiments.

The quasi-lacunae approach introduced in this paper can be considered an extension of our previous technique [25,24] based on the classical lacunae in the sense of Petrowsky. The current approach has a considerably wider applicability range though because of a key improvement in its design. Namely, it does not require the artificial solenoidal currents that guarantee the existence of classical lacunae in the solutions of Maxwell's equations. Similarly to the original lacunae-based approach of [24], the quasi-lacunae methodology can also be applied to the treatment of outer boundaries completely on its own, without having to be tied to any ABC or PML. This may require a wider buffer region around the computational domain than, say, an average PML would need. On the other hand, the shape of the boundary in this case can be quite general, and the methodology will remain provably free from any error associated with the grid truncation.

It should also be mentioned that some formulations may involve only one current (electric or magnetic), whereas the other current is zero.[6] In this case, the field with no current of its own will have genuine lacunae as opposed to quasi-lacunae. In turn, the discretization, at least on staggered grids, can be set up so that only the components of this field appear at the actual outer boundary. Therefore, a standard lacunae-based procedure of [25,24] can be applied, regardless of the possible non-solenoidal nature of the other current.

The decomposition of the original problem into the interior and auxiliary sub-problems discussed in Section 5 can, in fact, be considered a generalization of the electromagnetic equivalence theorem by Schelkunoff, see [41] or [12, Section 8.4]. The transition region $S\backslash S_\varepsilon$, see Fig. 2, on which the auxiliary sources $\mathbf{f}^{\text{aux}}$ of (31) are defined, can actually be taken as narrow as desired,[7] and in the limit can be reduced to the surface ∂S itself. Then, $\mu(\mathbf{x})$ becomes a step (Heaviside) function in the normal direction, and the auxiliary sources $\mathbf{f}^{\text{aux}}$ reduce to surface currents that shall formally be thought of as distributions, i.e., δ-layers on the surface. These surface currents will be the same as those that appear in the equivalence theorem, and the field they generate on the exterior region will be the same as the original field. Hence, the electromagnetic equivalence theorem can be obtained as a direct implication of the solvability and uniqueness results for Maxwell's equations. As mentioned in Section 1, there are publications in the literature that exploit the electromagnetic equivalence theorem in the computational context, see, e.g., [42–45].

Note also that a fair degree of flexibility exists when combining the interior and auxiliary sub-problems. For the purpose of matching the two solutions, there is no need to know the interior solution inside S except on the transition region $S\backslash S_\varepsilon$ because $\mu(\mathbf{x}) = 0$ on S_ε. Therefore, the two problems can, for example, be solved on two different grids. In doing so, the interior grid may need to be sophisticated to account for the geometry, while the exterior grid can have a much simpler structure. The two grids should overlap only in the vicinity of ∂S; they may either coincide (point-match) there or alternatively, once can interpolate between the grids (chimera strategy).

In our simulations, we computed the steady-state component of the overall solution by summing up the individual contributions generated by each partial problem in the course of its time-marching, see formula (61). This approach is straightforward and easy to implement, especially in the non-Huygens' setting of Section 5, but it formally takes us beyond Theorem 1, as the overall solution then includes the sum of an increasing number of individual static components. In practice, however, we still did not observe any long-time error accumulation, see Section 7, at least for those regimes that we have considered. This useful experimental observation indicates that a further theoretical analysis may be justified aimed at extending Theorem 1 to the case when only the currents are given, whereas the charges are not.

Another future direction is the development of an alternative version of the methodology that would involve independent solution of the Poisson equations (9) and (10) [or similar Poisson equations for the scalar electrostatic and magnetostatic potentials, which will be cheaper]. For convenience, the Poisson discretization can be built on the same grid, on which the Maxwell equations are discretized, and it shall guarantee at least the same order of accuracy. The ABC for the Poisson equation at the outer boundary ∂S can be obtained using Calderon's operators and the method of difference potentials, see [1]. This approach guarantees high accuracy of the boundary treatment and is very flexible as far as the geometry.

[6] There are no magnetic currents and no magnetic charges in genuine physics. Besides, the AP introduced in Section 5 for the analysis of non-Huygens' problems may also be driven by only one current.

[7] A relatively thin spherical transition zone defined by the function μ of (45) appears to have introduced no additional error in the Cartesian setting.

The Poisson problems need to be solved once per partition element. In other words, when the computational domain S falls completely into the quasi-lacuna for a given i [which happens at $t = t_2^{(i)}$, see formula (58b)], the steady-state component of the solution shall be recomputed. To do so, one uses the right-hand sides of Eqs. (9) and (10) given by the gradients of the charge densities accumulated by the given moment of time $t_2^{(i)}$.

Appendix A. Unsplit PML equations

Let $\mathbf{E}^{\text{aux}}$ and $\mathbf{H}^{\text{aux}}$ denote the auxiliary electric and magnetic fields, i.e., the solution to the AP of Section 6.2. According to [58], the modified Maxwell equations *inside the PML* can be written as follows:

$$\begin{aligned}
&-\frac{\partial H_y^{\text{aux}}}{\partial z} = \frac{1}{c}\frac{\partial E_x^{\text{PML}}}{\partial t} + \sigma_z E_x^{\text{PML}},\\
&\frac{\partial H_x^{\text{aux}}}{\partial z} = \frac{1}{c}\frac{\partial E_y^{\text{PML}}}{\partial t} + \sigma_x E_y^{\text{PML}},\\
&\frac{\partial H_y^{\text{aux}}}{\partial x} - \frac{\partial H_x^{\text{aux}}}{\partial y} = \frac{1}{c}\frac{\partial E_z^{\text{PML}}}{\partial t} + \sigma_y E_z^{\text{PML}},\\
&\frac{\partial E_z^{\text{aux}}}{\partial y} - \frac{\partial E_y^{\text{aux}}}{\partial z} = -\frac{1}{c}\frac{\partial H_x^{\text{PML}}}{\partial t} - \sigma_z H_x^{\text{PML}},\\
&\frac{\partial E_x^{\text{aux}}}{\partial z} - \frac{\partial E_z{}^{\text{aux}}}{\partial x} = -\frac{1}{c}\frac{\partial H_y^{\text{PML}}}{\partial t} - \sigma_x H_y^{\text{PML}}.
\end{aligned} \tag{64}$$

These equations are homogeneous since there are no currents beyond the computational domain$S$. Inside S, system (64) transforms into Eqs. (32)–(37) for $\mathbf{E}^{\text{aux}}$ and $\mathbf{H}^{\text{aux}}$ driven by the auxiliary currents $\mathbf{j}$ and $\mathbf{j}^{\text{M}}$. Compared to (32)–(37), system (64) contains five additional unknown variables, E_x^{PML}, E_y^{PML}, E_z^{PML}, H_x^{PML}, and H_y^{PML}, which are the functions of space (x, y, z) and time t. These functions coincide with the true auxiliary field components everywhere on S, but in the layer they may be different. They are governed by five additional ordinary differential equations in the PML:

$$\begin{aligned}
&\frac{1}{c}\frac{\partial E_x^{\text{aux}}}{\partial t} + \sigma_y E_x^{\text{aux}} = \frac{1}{c}\frac{\partial E_x^{\text{PML}}}{\partial t} + \sigma_x E_x^{\text{PML}},\\
&\frac{1}{c}\frac{\partial E_y^{\text{aux}}}{\partial t} + \sigma_z E_y^{\text{aux}} = \frac{1}{c}\frac{\partial E_y^{\text{PML}}}{\partial t} + \sigma_y E_y^{\text{PML}},\\
&\frac{1}{c}\frac{\partial E_z^{\text{aux}}}{\partial t} + \sigma_x E_z^{\text{aux}} = \frac{1}{c}\frac{\partial E_z^{\text{PML}}}{\partial t} + \sigma_z E_z^{\text{PML}},\\
&\frac{1}{c}\frac{\partial H_x^{\text{aux}}}{\partial t} + \sigma_y H_x^{\text{aux}} = \frac{1}{c}\frac{\partial H_x^{\text{PML}}}{\partial t} + \sigma_x H_x^{\text{PML}},\\
&\frac{1}{c}\frac{\partial H_y^{\text{aux}}}{\partial t} + \sigma_z H_y^{\text{aux}} = \frac{1}{c}\frac{\partial H_y^{\text{PML}}}{\partial t} + \sigma_y H_y^{\text{PML}}.
\end{aligned} \tag{65}$$

The sixth auxiliary function is identically equal to zero, $H_z^{\text{PML}} \equiv 0$, because of the symmetry, see Section 6.1. This allows us to drop the z-component of the Faraday law from system (64) that would otherwise be similar to Eq. (37) in the original Maxwell system.

The functions $\sigma_x = \sigma_x(x)$, $\sigma_y = \sigma_y(y)$, and $\sigma_z = \sigma_z(z)$ are the damping coefficients that facilitate the decay of the waves inside the PML in the directions x,y, and z, respectively. These functions are equal to zero everywhere on S^{aux} except in the layer, where they increase smoothly in the outward direction. For example, the quantity $\sigma_x = \sigma_x(x)$ is defined as follows:

$$\sigma_x(x) = \begin{cases} \sigma_0\left(\frac{x-a}{l}\right)^2, & x \geqslant a,\\ 0, & x < a. \end{cases}$$

For the PML of width $l = 0.75$ cm we take $\sigma_0 = 10$.

It is to be noted that the Cartesian PML Eqs. (64) and (65) differ for different parts of the layer that surrounds the computational domain. Specifically, there is a difference between the so-called face-PML, edge-PML, and corner-PML regions, see Fig. 11. In general, the PML is supposed to provide for a perfect matching between the layer and the interior of the computational domain, and also guarantee a sufficient attenuation of the outgoing waves. However, in the face-PML region it is sufficient to have the decay of the field in only one direction — normal to the boundary, whereas the equations in the edge-PML region and the corner-PML region are designed in a more complicated way so that to provide for a field decay in two and three orthogonal directions simultaneously. It is the edge-PML and corner-PML regions that appear prone to the long-term error buildup.

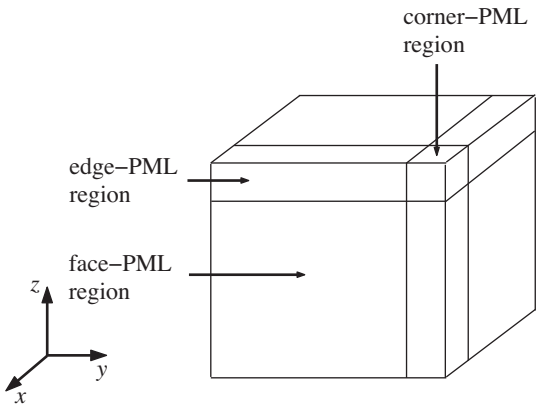

Fig. 11. PML regions.

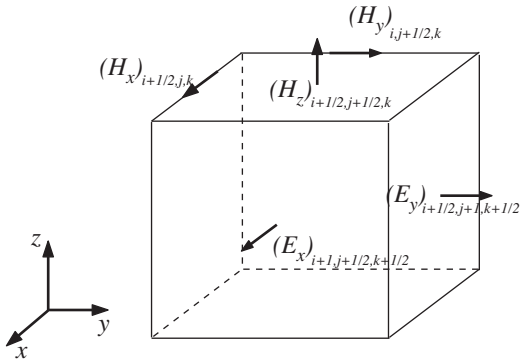

Fig. 12. Allocation of the field components on an elementary cell for the Yee scheme [9].

Appendix B. The Yee scheme

In the Yee scheme [9], the field components are staggered on the grid in both space and time. The field allocation on an elementary spatial cell is shown in Fig. 12.

As by now the Yee scheme has become the "industry standard," see [12], we write out explicitly only two discrete equations that we will need for further discussion — the counterparts of Eqs. (34) and (35):

$$\frac{(H_y)^{n+1/2}_{i+1,j+1/2,k}-(H_y)^{n+1/2}_{i,j+1/2,k}}{h_x}-\frac{(H_x)^{n+1/2}_{i+1/2,j+1,k}-(H_x)^{n+1/2}_{i+1/2,j,k}}{h_y}=\frac{1}{c}\frac{(E_z)^{n+1}_{i+1/2,j+1/2,k}-(E_z)^{n}_{i+1/2,j+1/2,k}}{\tau}+\frac{4\pi}{c}(j_z)^{n+1/2}_{i+1/2,j+1/2,k}, \tag{66}$$

$$\frac{(E_z)^{n+1}_{i+1/2,j+1/2,k}-(E_z)^{n+1}_{i+1/2,j-1/2,k}}{h_y}-\frac{(E_y)^{n+1}_{i+1/2,j,k+1/2}-(E_y)^{n+1}_{i+1/2,j,k-1/2}}{h_z}=-\frac{1}{c}\frac{(H_x)^{n+3/2}_{i+1/2,j,k}-(H_x)^{n+1/2}_{i+1/2,j,k}}{\tau}. \tag{67}$$

Here the subscripts i,j, and k (and the semi-integers) correspond to the spatial variables x,y, and z, respectively, whereas the superscript n and the semi-integers correspond to the time variable t. As the scheme is explicit, the time step τ must satisfy the Courant stability constraint, and in our computations we typically choose $\tau = 0.2h$.

The case of $i = 0$, $j = 0$, or $k = 0$ requires a minor modification of the discrete equations. When, for example, $i = 0$ (which corresponds to the plane $x = 0$), the symmetry relation (42) shall be exploited, i.e., $H_y(0,y,z) = 0$, and the first term on the left-hand side of Eq. (66) transforms into

$$\frac{(H_y)^{n+1/2}_{1,j+1/2,k}-(H_y)^{n+1/2}_{0,j+1/2,k}}{h_x}\mapsto\frac{(H_y)^{n+1/2}_{1,j+1/2,k}}{h_x}.$$

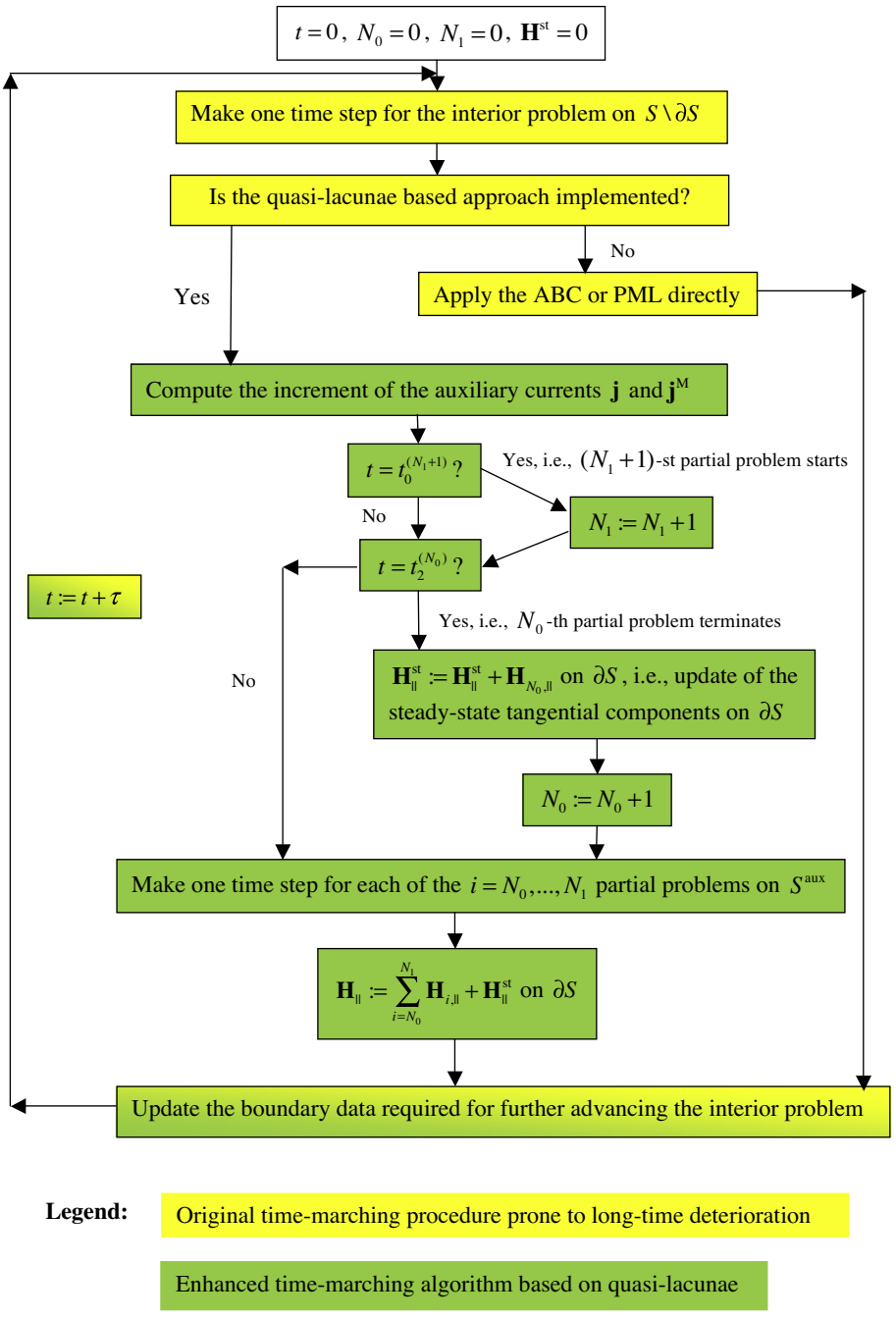

Fig. 13. Block diagram of the algorithm. $\mathbf{H}_{\|}$, $\mathbf{H}_{i,\|}$, and $\mathbf{H}_{\|}^{st}$ are the tangential components of the total, partial # i, and steady-state magnetic field. The electric field is not shown explicitly for brevity.

Similar symmetry-based considerations apply to the other two boundary planes, $y = 0$ and $z = 0$, and to the remaining discrete equations.

References

[1] S.V. Tsynkov, Numerical solution of problems on unbounded domains. A review, Appl. Numer. Math. 27 (4) (1998) 465–532.
[2] T. Hagstrom, Radiation boundary conditions for the numerical simulation of waves, Acta Numerica 8 (1999) 47–106.
[3] O.M. Ramahi, Stability of absorbing boundary conditions, IEEE Trans. Antennas Propagat. 47 (1999) 593–599.
[4] J. Diaz, P. Joly, An analysis of higher order boundary conditions for the wave equation, SIAM J. Appl. Math. 65 (5) (2005) 1547–1575 (electronic).

[5] T. Hagstrom, T. Warburton, Complete radiation boundary conditions: minimizing the long time error growth of local methods, SIAM J. Numer. Anal. 47 (5) (2009) 3678–3704.
[6] J.-P. Bérenger, A perfectly matched layer for the absorption of electromagnetic waves, J. Comput. Phys. 114 (2) (1994) 185–200.
[7] J.-P. Bérenger, Three-dimensional perfectly matched layer for the absorption of electromagnetic waves, J. Comput. Phys. 127 (2) (1996) 363–379.
[8] S. Abarbanel, D. Gottlieb, A mathematical analysis of the PML method, J. Comput. Phys. 134 (2) (1997) 357–363.
[9] K.S. Yee, Numerical solution of initial boundary value problem involving Maxwell's equations in isotropic media, IEEE Trans. Antennas Propagat. 14 (1966) 302–307.
[10] S. Abarbanel, D. Gottlieb, J.S. Hesthaven, Long time behavior of the perfectly matched layer equations in computational electromagnetics, J. Sci. Comput. 17 (1–4) (2002) 405–422.
[11] S. Abarbanel, H. Qasimov, S. Tsynkov, Long-time performance of unsplit PMLs with explicit second order schemes, J. Sci. Comput. 41 (1) (2009) 1–12.
[12] A. Taflove, S.C. Hagness, Computational Electrodynamics: The Finite-Difference Time-Domain Method, third ed., Artech House Inc., Boston, MA, 2005.
[13] R.L. Wagner, W.C. Chew, An analysis of Liao's absorbing boundary conditions, J. Electromagn. Waves Appl. 9 (1995) 993–1009.
[14] O.M. Ramahi, Stable FDTD solutions with higher-order absorbing boundary conditions, Microwave Opt. Technol. Lett. 15 (1995) 132–134.
[15] S.D. Gedney, The perfectly matched layer absorbing medium, in: A. Taflove (Ed.), Advances in Computational Electrodynamics: The Finite-Difference Time-Domain Method, Artech House, Boston, MA, 1998, pp. 263–340.
[16] J.A. Roden, S.D. Gedney, Convolution PML(CPML): an efficient FDTD implementation of the CFS–PML for arbitrary media, Microwave Opt. Technol. Lett. 27 (5) (2000) 334–339.
[17] E. Bécache, P.G. Petropoulos, S.D. Gedney, On the long-time behavior of unsplit perfectly matched layers, IEEE Trans. Antennas Propagat. 52 (5) (2004) 1335–1342.
[18] S. Abarbanel, D. Gottlieb, J.S. Hesthaven, Non-linear PML equations for time dependent electromagnetics in three dimensions, J. Sci. Comput. 28 (2–3) (2006) 125–137.
[19] S.V. Petropavlovsky, S.V. Tsynkov, Quasi-lacunae of Maxwell's equations, SIAM J. Appl. Math. 71 (4) (2011) 1109–1122. <http://dx.doi.org/10.1137/100798041>.
[20] I. Petrowsky, On the diffusion of waves and the lacunas for hyperbolic equations, Mat. Sbornik (Recueil Math.) 17(59) (3) (1945) 289–370.
[21] V.S. Ryaben'kii, S.V. Tsynkov, V.I. Turchaninov, Long-time numerical computation of wave-type solutions driven by moving sources, Appl. Numer. Math. 38 (2001) 187–222.
[22] V.S. Ryaben'kii, S.V. Tsynkov, V.I. Turchaninov, Global discrete artificial boundary conditions for time-dependent wave propagation, J. Comput. Phys. 174 (2) (2001) 712–758.
[23] S.V. Tsynkov, Artificial boundary conditions for the numerical simulation of unsteady acoustic waves, J. Comput. Phys. 189 (2) (2003) 626–650.
[24] S.V. Tsynkov, On the application of lacunae-based methods to Maxwell's equations, J. Comput. Phys. 199 (1) (2004) 126–149.
[25] H. Qasimov, S. Tsynkov, Lacunae based stabilization of PMLs, J. Comput. Phys. 227 (2008) 7322–7345.
[26] T. Ha-Duong, P. Joly, On the stability analysis of boundary conditions for the wave equation by energy methods. I. The homogeneous case, Math. Comput. 62 (206) (1994) 539–563, doi:10.2307/2153522. <http://dx.doi.org.prox.lib.ncsu.edu/10.2307/2153522>.
[27] D. Baffet, D. Givoli, On the stability of the high-order Higdon absorbing boundary conditions, Appl. Numer. Math. 61 (2011) 768–784.
[28] A. Ditkowski, Private Communication, Tel Aviv University, Israel, 2011.
[29] M. Born, E. Wolf, Principles of Optics: Electromagnetic Theory of Propagation, Interference and Diffraction of Light, With Contributions by A.B. Bhatia, P.C. Clemmow, D. Gabor, A.R. Stokes, A.M. Taylor, P.A. Wayman, W.L. Wilcock, seventh (expanded) ed., Cambridge University Press, Cambridge, 1999.
[30] M.J.M. Jessel, Sur les absorbeurs actifs, in: Proceedings of 6th ICA, Tokio, 1968, p. 82 (Paper F-5-6).
[31] M.J.M. Jessel, G.A. Mangiante, Active sound absorbers in an air duct, J. Sound Vibr. 23 (3) (1972) 383–390.
[32] G.A. Mangiante, Active sound absorption, J. Acoust. Soc. Am. 61 (6) (1977) 1516–1523.
[33] G. Canevet, Active sound absorption in an air conditioning duct, J. Sound Vibr. 58 (3) (1978) 333–345.
[34] M.J.M. Jessel, Some evidences for a general theory of active noise sound absorption, in: Inter-Noise 79: Proceedings, Institute of Fundamental Technological Research of the Polish Academy of Sciences, Warsaw, Poland, 1979, pp. 169–174.
[35] G. Mangiante, The JMC method for 3-D active sound absorption: a numerical simulation, Noise Control Eng. J. 41 (2) (1993) 339–345.
[36] S. Uosukainen, Modified JMC method in active control of sound, Acta Acustica united with Acustica 83 (1) (1997) 105–112.
[37] S. Uosukainen, Active sound scatterers based on the JMC method, J. Sound Vibr. 267 (5) (2003) 979–1005.
[38] H. Lim, S.V. Utyuzhnikov, Y.W. Lam, A. Turan, M. Avis, V.S. Ryaben'kii, S.V. Tsynkov, An experimental validation of the noise control methodology based on difference potentials, AIAA J. 47 (4) (2009) 874–884.
[39] S. Charles, S. Kapotas, S. Phadke, Absorbing boundaries with Huygens' secondary sources, in: Proceedings of 64th Annual S.E.G. Meeting, Los Angeles, USA, 1994, pp. 1363–1366.
[40] G. Mangiante, S. Charles, Absorbing boundary conditions for acoustic waves and Huygens' principle, J. Acoust. Soc. Am. 103 (5) (1998) 2971.
[41] S.A. Schelkunoff, Some equivalence problems of electromagnetics and their application to radiation problems, Bell Syst. Tech. J. 15 (1) (1936) 92–112.
[42] J.-P. Bérenger, A Huygens subgridding for the FDTD method, IEEE Trans. Antennas Propagat. 54 (12) (2006) 3797–3804.
[43] J.-P. Bérenger, Extension of the FDTD Huygens subgridding algorithm to two dimensions, IEEE Trans. Antennas Propagat. 57 (12) (2009) 3860–3867.
[44] F. Costen, J.-P. Bérenger, Extension of the FDTD Huygens subgridding to frequency dependent media, Annal. Telecommun. 65 (3) (2010) 211–217.
[45] J.-P. Bérenger, On the Huygens absorbing boundary conditions for electromagnetics, J. Comput. Phys. 226 (1) (2007) 354–378, doi:10.1016/j.jcp.2007.04.008. <http://dx.doi.org/10.1016/j.jcp.2007.04.008>.
[46] L. Gårding, Sharp fronts and lacunas — some problems and results, in: N.H. Ibragimov, L.V. Ovsyannikov (Eds.), Proceedings of the Joint IUTAM/IMU Symposium Group-Theoretical Methods in Mechanics, USSR Acad. Sci., Siberian Branch, Institute of Hydrodynamics — Computing Center, USSR, Novosibirsk, 1978, pp. 130–144.
[47] H.A. Warchall, Wave propagation at computational domain boundaries, Commun. Partial Diff. Eqs. 16 (1) (1991) 31–41, doi:10.1080/03605309108820750. <http://dx.doi.org/10.1080/03605309108820750>.
[48] H.A. Warchall, Induced lacunas in multiple-time initial value problems and unbounded domain simulation, in: J. Weiner, J.K. Hale (Eds.), Partial Differential Equations, Pitman Research Notes in Mathematics Series, vol. 273, Longman Scientific & Technical, Essex, England, 1992, pp. 258–264.
[49] L.D. Landau, E.M. Lifshitz, Course of Theoretical Physics, The Classical Theory of Fields, fourth ed., vol. 2, Pergamon Press, Oxford, 1975 (translated from the Russian by Morton Hamermesh).
[50] L.D. Landau, E.M. Lifshitz, Course of Theoretical Physics, Electrodynamics of Continuous Media, vol. 8, Pergamon International Library of Science, Technology, Engineering and Social Studies, Pergamon Press, Oxford, 1984 (translated from the second Russian edition by J.B. Sykes, J.S. Bell and M.J. Kearsley, Second Russian edition revised by Lifshits and L.P. Pitaevskii).
[51] V.S. Vladimirov, Equations of Mathematical Physics, Dekker, New-York, 1971.
[52] R. Courant, D. Hilbert, Methods of Mathematical Physics, vol. II, Wiley, New York, 1962.
[53] E.T. Meier, A.H. Glasser, V.S. Lukin, U. Shumlak, Modeling open boundaries in dissipative MHD simulation, J. Comput. Phys., submitted for publication.
[54] T. Hagstrom, M.L. De Castro, D. Givoli, D. Tzemach, Local high-order absorbing boundary conditions for time-dependent waves in guides, J. Comput. Acoust. 15 (1) (2007) 1–22.
[55] T. Hagstrom, A. Mar-Or, D. Givoli, High-order local absorbing conditions for the wave equation: extensions and improvements, J. Comput. Phys. 227 (6) (2008) 3322–3357.

[56] E. Bécache, D. Givoli, T. Hagstrom, High-order absorbing boundary conditions for anisotropic and convective wave equations, J. Comput. Phys. 229 (4) (2010) 1099–1129.
[57] E. Bécache, P. Joly, On the analysis of Bérenger's perfectly matched layers for Maxwell's equations, M2AN Math. Model. Numer. Anal. 36 (1) (2002) 87–119.
[58] L. Zhao, A.C. Cangellaris, GT-PML: generalized theory of perfectly matched layers and its application to the reflectionless truncation of finite-difference time-domain grids, IEEE Trans. Microwave Theory Tech. 44 (1996) 2555–2563.
[59] F.L. Teixeira, W.C. Chew, PML-FDTD in cylindrical and spherical grids, IEEE Microwave Guided Wave Lett. 7 (9) (1997) 285–287.